MOST INFLUENTIAL VARIABLES FOR SOLAR RADIATION FORECASTING USING ARTIFICIAL NEURAL NETWORKS

by

Bader M. Alluhaidah

Submitted in partial fulfilment of the requirements
for the degree of Master of Applied Science

at

Dalhousie University
Halifax, Nova Scotia
June 2014

Dedication

Words cannot express the gratitude I feel for the nurturing and support that my parents have provided me in this life,

It is my sincere hope that they are as proud of their son as their son is of them

Table of Contents

List of Tables

List of Figures

Abstract

Decaying fossil fuel resources, international relation complexities, and the risks associated with nuclear power have led to an increased demand for alternative energy sources. Renewable energy sources offer adequate solutions to these challenges.

Forecasting of solar energy has also increased over the past decade due to its use in photovoltaic (PV) system design, load balance in hybrid systems, and projected potential future PV system feasibility. Artificial neural networks (ANN) have been used successfully for solar energy forecasting. In this work, several meteorological variables from Saudi Arabia as a case study will be used to determine the most effective variables on Global Solar Radiation (GSR) prediction. Those variables will be used as inputs for a proposed GSR prediction model. This model will be applicable in different locations and conditions. This model has a simple structure and offers better results in terms of error between actual and predicted solar radiation values.

List of Abbreviations and Symbols Used

ANN	artificial neural network
cc	cloud-cover
d	the day
GSR	global solar radiation
GSR_{avg}	average global solar radiation
H	relative humidity
L_{al}	altitude
L_{la}	latitude
L_{lo}	longitude
M	the month
$MAPE$	mean absolute percentage of error
MLP	multilayer perceptron
P	pressure
r	coefficient of correlation
R^2	coefficient of determination
$RMSE$	root mean square error
S_m	measured daily sunshine duration
S_t	theoretical daily sunshine duration
T	daily average air temperature
T_{max}	daily maximum air temperature
w_d	wind-direction
w_s	wind-speed

Acknowledgements

My unreserved gratitude and praises are for Allah, the Most Compassionate, and the Most Merciful. He blessed me with his bounties, and he has given me the strength and courage to reach my goals during the course of this research.

I must also thank Qassim University for providing me a scholarship. I truly appreciate the people at Saudi Cultural Bureau in Canada who have been very helpful in the administration of my scholarship.

I would like to thank my supervisor, Dr. El-hawary, for his guidance, help and support throughout my research. I also appreciate his patient encouragement and valuable advice over the course of my entire Master program.

I wish to acknowledge Dr. Jason Gu and Dr. William Phillips for serving on my supervisory committee.

I would also like to thank Shadi Shehadeh and Aaron MacNeill, PhD candidates in the Power Group, for numerous fruitful discussions and useful suggestions for my work.

Thanks also go to my friends and colleagues, especially Dr. Hamed Aly, without whom I could not have succeeded in my endeavours.

Special thanks go to my family, especially my brothers and my sister, whom I have missed these many years, being away from home.

I would especially like to thank the person who has endured the hardship of my absence, and put up with my constant urgency to complete my work. I express heartfelt, unending gratitude to my wife, Assma Alsalloomi, the mother of my sons, Alwaleed and Talal, for being a pillar of support standing firm beside me throughout this journey.

Finally, I would like to express my sincere love and gratitude to my parents, Mohammad and Norah. I owe them more than anyone could possibly imagine, notwithstanding my academic achievements. I thank them for their love and infinite care, which has made the person I am today.

Chapter 1: Introduction

Electric power consumption has significantly increased in recent decades. Traditional energy, such as oil, coal and nuclear, has a negative impact on the environment. For these reasons, researchers have turned toward renewable sources such as solar, wind and marine energy. Renewable energy is characterized as clean and durable energy. Scientists are trying to improve the efficiency of converting this energy into electricity.

Solar energy production has dramatically increased in the past decade. The world's capacity of total installed solar power generation capacity has increased from almost 2 GW in 2002 to more than 100 GW at the end of 2012 [1]. Power fluctuation is one of the challenges facing the implementation of solar energy due to the intermittency and variability of solar radiation. Prediction using artificial intelligence (AI) techniques is used to overcome these challenges.

1.1 Thesis Objective

The objective of this research is to find a model that predicts solar radiation by building the appropriate ANN model using the best set of weather variables as inputs. This model helps to achieve better results in terms of error values, between actual and predicted data, and in terms of structural simplicity, the number of neurons, lyres, and inputs of the model. In addition, this research seeks to determine the best number of internal ANN units (neurons.)

1.2 Thesis Contribution

In this work, the ANN model is proposed for solar radiation prediction. A thorough analysis and simulation are presented and discussed. A Matlab^{TM} code is implemented to model the suggested structure. The author's contribution to this work includes carrying out numerical simulations and comparing the results with other models in the solar radiation prediction field. In addition, the optimum number of neurons for each ANN model considered. In particular, this thesis discovered that increasing the number of neurons in an ANN does not necessarily improve prediction accuracy.

1.3 Thesis Outline

This thesis is organized as follows:

Chapter 2 introduces a brief overview of solar energy and its development history. The technologies of converting solar energy into electricity are discussed. The PV system types, grid-connected and stand-alone (off-grid), are explained.

Chapter 3 reviews the effect of the atmosphere on solar radiation and also introduces the world-wide distribution of solar radiation in the world. Detailed information about solar radiation and power in Saudi Arabia are discussed in this chapter.

Chapter 4 discusses the model that is applied in this thesis: the artificial neural network. It also introduces a literature review of solar radiation prediction approaches.

Chapter 5 discusses the Global Solar Radiation (GSR) prediction models and results, and compare them with other models.

Finally, Chapter 6 presents the conclusions of the research and proposes a basis for future work in this field.

Chapter 2: Solar Energy Technologies

This chapter provides a brief overview of solar energy, solar energy conversion technologies, and typically implemented solar energy systems.

2.1 Introduction

Solar energy can be defined as the energy produced from the Sun's radiation. This energy comes in two forms, heat and light. Since solar energy comes from the sun it is considered a renewable source of energy because nothing is consumed to use this energy. Solar energy is also a clean source of energy that does not damage the environment with harmful emissions or waste like other source such as nuclear and conventional energy. Solar energy sources can be located anywhere where there is sunlight, thus solar energy sites can be constructed close to where consumers are located; this could potentially reduce transmission and distribution costs. The availability of solar energy sources could also help societies achieve political and economic independence [2, 3].

A drawback to using solar energy is that it is dependent on weather variables such as air pollution, wind velocity, and cloud cover. This weather variability makes solar energy potentially unreliable. Another drawback of solar energy is its high initial installation cost [2, 4].

2.2 Solar Energy

Solar energy has been used since ancient times as a source of light and heat. The beginning of the new age of solar energy technology started in the 18th century. In 1767, Horace de Saussure invented the first solar collector, which was a box surrounded by three layers of glass to absorb thermal energy. In 1839, Edmond Becquerel discovered

the photovoltaic effect, which is the conversion of solar radiation into electric current in a material [5]. In 1876, William Grylls Adams and Richard Evans Day proved that a solid material can convert light into electricity without additional heating or moving parts. In 1891, Clarence Kemp created the first commercial solar water heater. In 1908, William J. Bailley, created a solar collector which was made of copper coils and an insulated box. His discovery is the basis for manufacturing today's equipment. After the Second World War, solar powered equipment became more popular in the United States [6]. Since 1958, solar energy has been used in space equipment. The efficiency and cost of solar cells was improved in the 1970's. The United States government along with many others have launched solar energy research labs and institutes [5]. In the early 1980's, the first solar power aircraft and car were created [7]. In the late 1980's, large-scale solar power plants were designed and built [7]. In 2013, solar power plants were capable of producing over 200 Megawatts of power. The total installed solar power generation capacity increased to more than 100 GW by the end of 2012 from an almost 2.2 GW capacity in the early nineties [1]. Figure 2-1 shows the world total installed PV power.

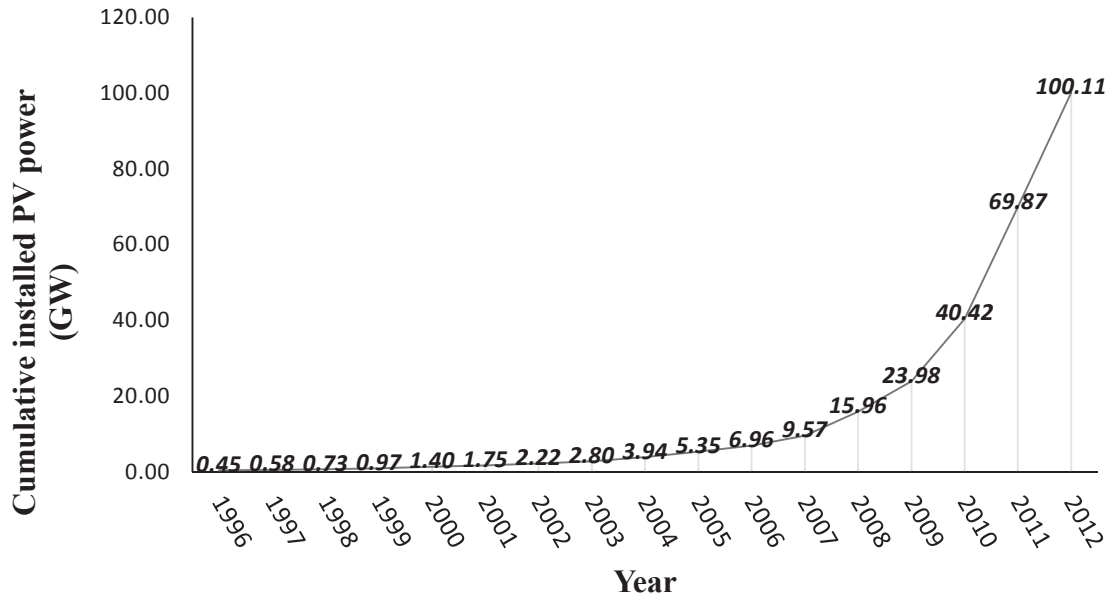

Figure 2-1 Total World Installed PV

This figure shows that there is a significant increase in PV power installations every year. Also noteworthy is how the increasing trend of installing PV systems significantly began in 2006.

2.3 Solar Energy Technologies

Solar energy can be harvested and converted into electricity through the use of two main technologies. These technologies include solar-thermal power generation and photovoltaic (PV) power generation.

2.3.1 Solar Thermal Technology

Solar-thermal energy technology focuses the sun's radiation to generate heat. This heat can be used directly for the following applications: agricultural drying, solar air heaters, solar water heaters, solar cooling systems, and solar cookers. This generated heat can also

be used to spin turbines on electrical generators. Figure 2-2 provides an example of what a solar-thermal generation site would consist of [8].

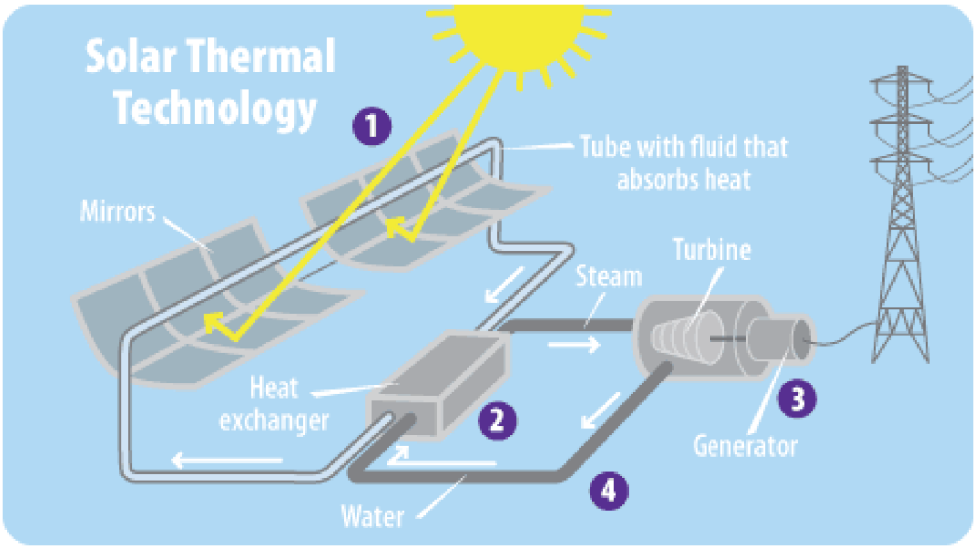

Figure 2-2 Solar Thermal Technology [8]

2.3.2 Photovoltaic Cells

Photovoltaic (PV) cell technology converts light incident on a material into electrical energy. PV cell materials are composed mainly of silicon and other semiconductor materials. The incident light excites the electrons in the semiconductor, which in turn increases the semiconductor conductivity and produces a direct current (DC) flow [9]. Figure **2-3** provides an overview of this energy conversion process.

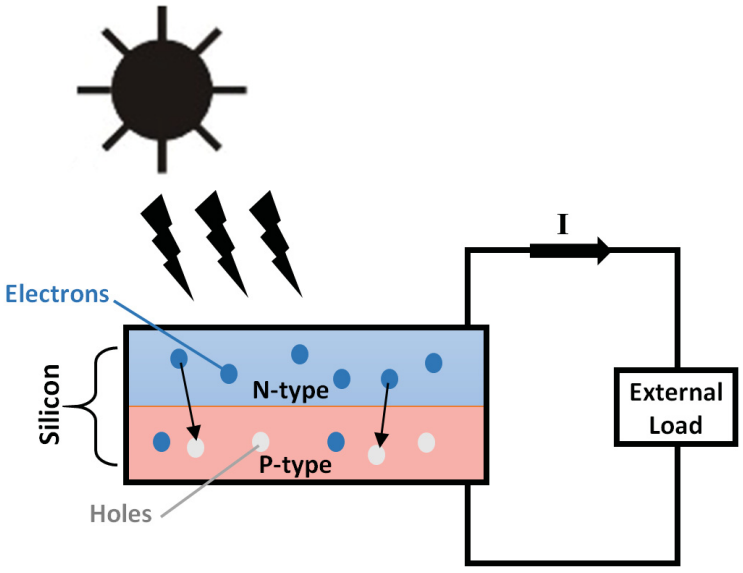

Figure 2-3 Photovoltaic Cell Operation

The equivalent circuit for a PV cell can be seen in Figure 2-4 [10]. There are two main types of PV technology: crystalline silicon-based PV cells and thin film. Thin film technology is made from various semi-conductor materials such as cadmium-telluride, amorphous silicon, and copper indium gallium diselenidel [10].

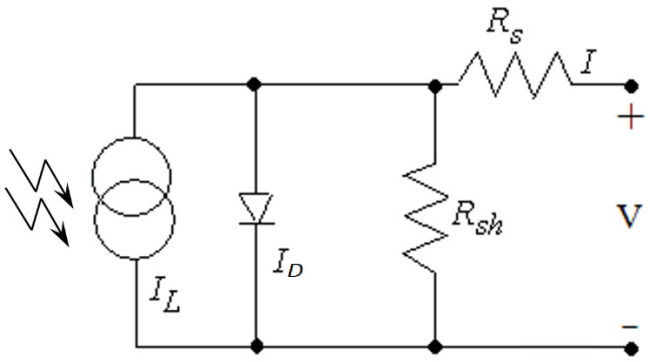

Figure 2-4 PV Cell Equivalent Circuit [10]

A well-known general equation for the diode current of the PV cell is given by [10]:

$$I = I_L - I_D \left[e^{\frac{Q(V+IR_{sh})}{nkT}} - 1 \right] - \frac{V + IR_s}{R_{sh}} \quad (2.1)$$

where

I is the overall diode current produced by the cell

I_L is the current generated by the incident light at the cell

I_D is the reverse saturation current of the diode

Q is the electron charge ($1.60217646 \times 10^{-19}\ C$)

n is the ideality factor

k is the Boltzmann constant ($1.3806503 \times 10^{-23} J/K$)

T is the temperature of the PV cell measured in degrees Kelvin

V is the voltage across the cell.

PV systems mainly consist of PV cells which are connected in a series and/or parallel to form a PV module, and a PV panel consists of a group of PV modules. A group of PV panels are arranged to structure a PV array [10]. The second component of a PV system is the converter, which is used to regulate the output of PV cells and/or convert the generated voltage waveforms from DC to AC [11]. More components can be added to the system depending on the requirements and application, such as: batteries, control and synchronization units. These components are added in applications such as a multi-source or a grid-connected system.

2.4 PV System Classification

PV systems can be classified into two categories: grid-connected and stand-alone (off-grid) systems [12, 13]. These systems are further explained in the following sections. Figure 2-5 shows a chart outlining all of the potential PV system topologies.

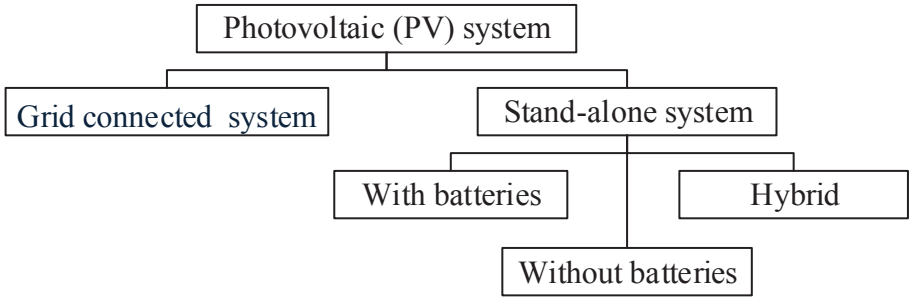

Figure 2-5 PV System Topologies

2.4.1 PV Stand-Alone System

The stand-alone system is divided into three categories: with batteries, without batteries, and a hybrid system. When the installation cannot be feasibly or practically connected to a grid the stand-alone system is the best option [14].

Batteries are added to the stand-alone system when the power demand is greater than the power supplied by the system. Since solar radiation is not available all the time, such as nighttime or cloudy days, batteries become one of the best solutions for maintaining load demands. Batteries store the extra-generated power when solar radiation is abundant such that the energy can be used when solar radiation is not available. Stand-alone systems with batteries are usually applied in rural areas where it is difficult to connect to the grid [15].

The hybrid stand-alone system is more complicated and advanced than the stand-alone system. This system is connected to another renewable energy system or traditional generators. Hybrid systems mainly are connected to wind turbines, diesel generators, and traditional power generating units. More units, such as a converter and control unit, are added to the hybrid system [16, 17]. Figure 2-6 shows a general diagram of a stand-alone PV system.

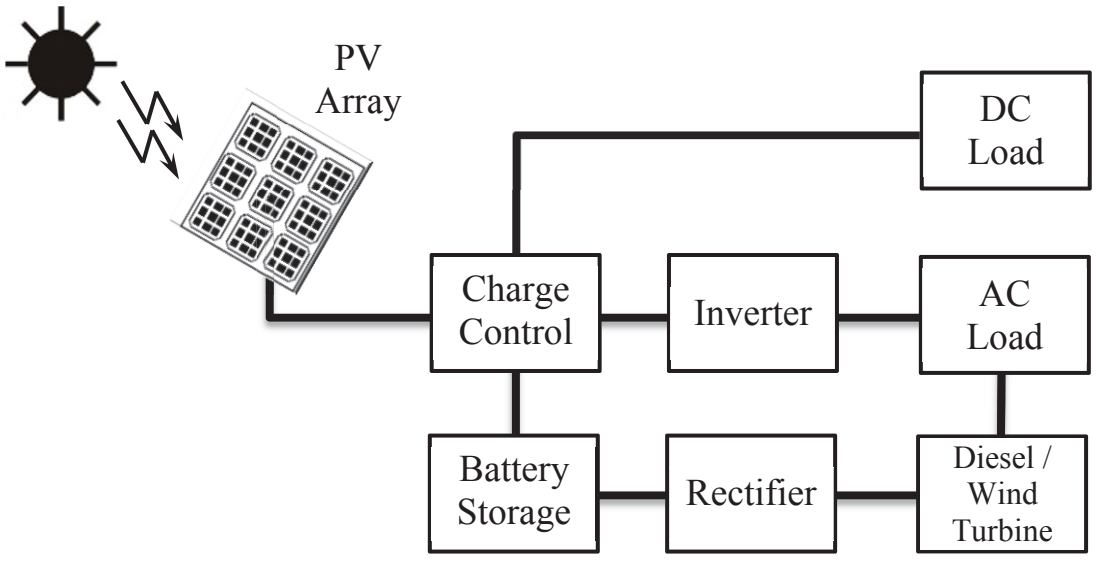

Figure 2-6 Stand-Alone PV System Topology

2.4.2 Grid Connected System

The grid-connected system is the PV stand-alone system connected to the utility power lines. This kind of system has become more popular in recent years. It is a more complex system than the stand-alone systems. Synchronization, control and metering units are added to these types of systems [18, 19]. Figure **2-7** shows a general diagram of grid-connected PV system.

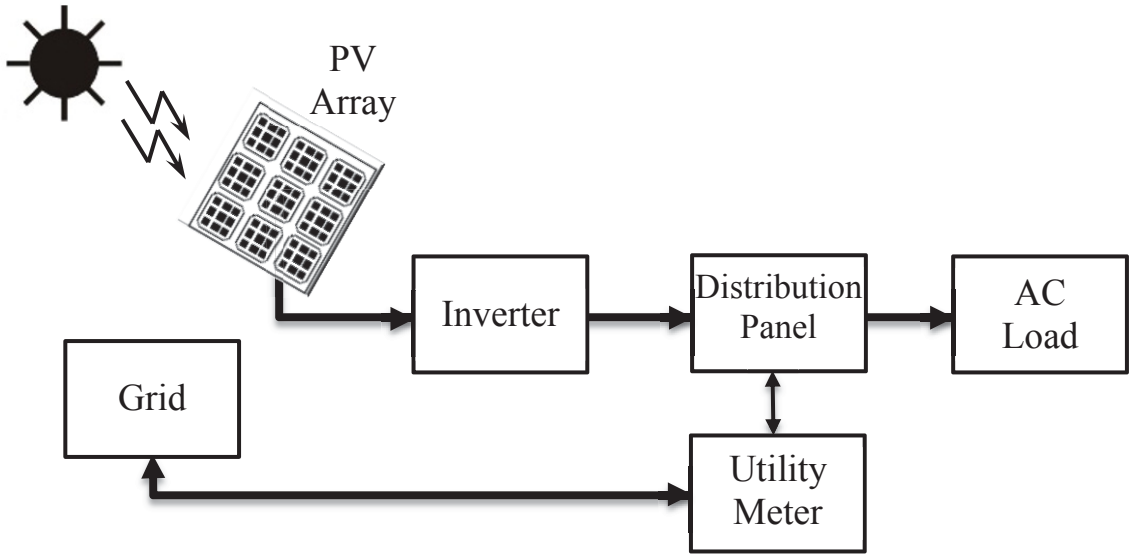

Figure 2-7 Grid-Connected PV System

Grid connected systems have many advantages over the other PV systems. When the PV system cannot supply the load's demand, the control unit allows for power from the grid to support the PV system in meeting that demand. When the PV system has more power than the load requires the control unit transfers the extra power to the grid, making it a more reliable source of energy. The ability to meet the load's demand, economic benefits, and environmental considerations make the grid-connected PV system a more popular choice [20].

Chapter 3: Distribution of Solar Energy

This chapter provides a brief overview of solar energy throughout the world and in comparison to Saudi Arabia.

3.1 Introduction

Solar radiation is electromagnetic radiation emitted from the sun. Solar radiation can be defined as the total amount of quantum energy produced by incident photons per unit of area. Solar radiation can be expressed in Joules per square meter J/m^2 or watt—hours per square meter $\frac{1}{3600} Wh/m^2$. This value of incident energy on the earth's surface depends on factors such as location, air pollution, and cloud cover [21].

Photons in solar beams interact and penetrate the atmosphere in four ways. The first kind of interaction is where photons are reflected back into space due to the interaction with the atmosphere and Earth. Second, the photons are absorbed by the Earth's atmosphere. Third, photons are scattered to produce diffuse radiation, which is a significant factor in solar power applications and forecasting. Finally, the remaining photons unabsorbed, un-scattered, and un-reflected are called direct radiation which is the most important factor in solar power applications and forecasting. Figure 3-1 displays these four cases of photons penetrating the atmosphere. The atmospheric losses of the extraterrestrial solar energy can reach 30% on a very clear day and can reach 100% on a very cloudy day [22, 23].

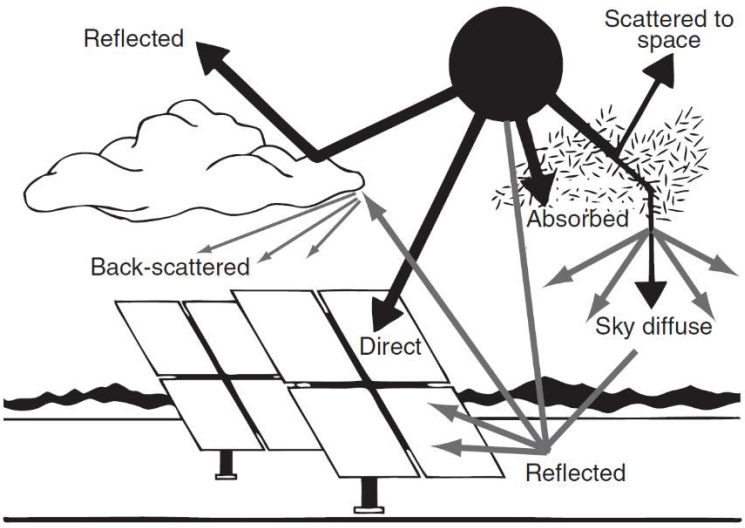

Figure 3-1 Solar Radiation Atmospheric Interaction [23]

The total solar radiation incident on a horizontal surface is called a Global Horizontal Irradiance (GHI) and equals the sum of direct solar radiation (Direct Normal Irradiance (DNI)) and Diffuse Horizontal Irradiance (DHI). GHI can be expressed as [24]:

$$GHI = DHI + DNI \cdot \cos(z) \tag{3.1}$$

where z is the solar zenith angle.

3.2 Solar Radiation in the World

The Earth's solar radiation distribution can be divided into three regions. Figure 3-2 shows the solar radiation distribution throughout the world. Due to the variations in climate between regions of the world significant differences of solar radiation are expected.

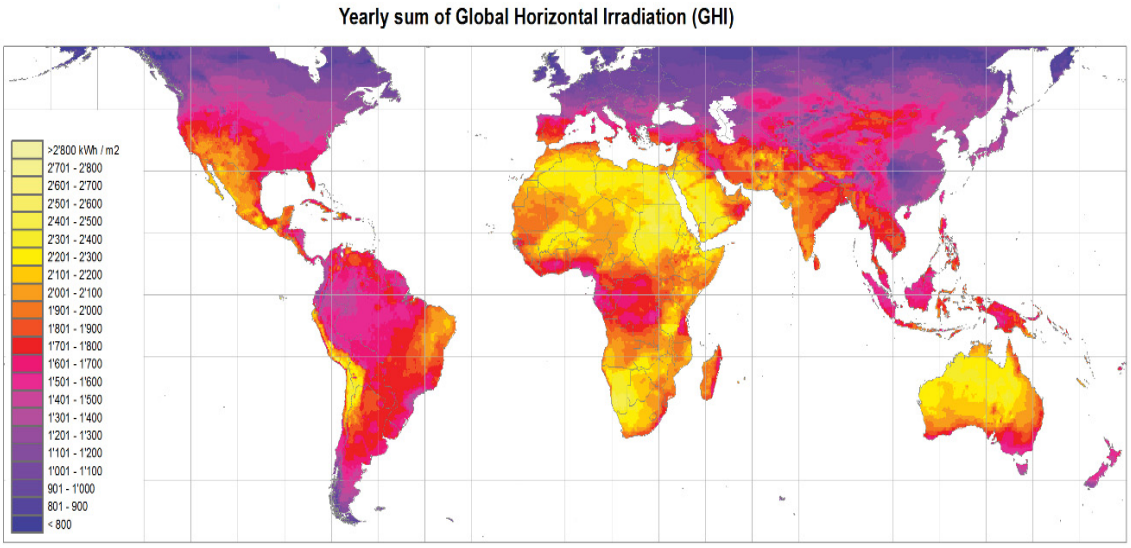

Figure 3-2 World Solar Radiation Intensity [25]

The first region, which has the highest amount of solar radiation, lies between latitudes 15°N, and 35°N. Most of this solar radiation comes from direct radiation, as there is a lack of cloud cover and rainfall. The second region lies between latitude 15°N and 0°N. This region has the second highest level of solar radiation. This region has higher levels of diffuse radiation due to humidity and cloud cover. In this region, there is almost a constant amount of solar radiation during the year. The third region located above 35°N has the lowest level of solar radiation. This is due to the cloud cover. Almost half of the radiation in this region comes from diffusion radiation. The solar radiation is lowest at the Earth's poles [26].

3.3 Solar Radiation and Power Generation in Saudi Arabia

Saudi Arabia has a significant supply of solar radiation. As such, it is in the country's best interest to harness this renewable source of power generation. Currently there are many solar generation sites under development.

3.3.1 Solar Radiation in Saudi Arabia

Saudi Arabia (SA) is located in the southwest of Asia between latitudes 17.5˚N and 31˚N and longitudes 36.6˚E and 50˚E [27]. It has a total area of 2,250,000 km², which is about 80% of the Arabian Peninsula [28]. As of 2012 the total population of Saudi Arabia is 28.3M with an average annual growth rate of 1.9% [29].

Aridity and extreme temperatures characterize the climate in SA with the exception of the coastal region, which has high humidity coupled with more moderate temperatures. In the middle of SA, the average summer daytime temperature could reach 45°C and it is not unusual for temperatures to reach 54°C. However, in winter, it seldom drops freezing. The average amount of rainfall in SA is very low except in the southwestern region. This region experiences monsoons, which can bring an average of 300 millimeters of precipitation between October and March [28].

Saudi Arabia has the largest global oil reserves in the world. This represents one-fifth of the global oil reserves. SA also has the world's fifth largest natural gas reserves [30]. In addition, as mentioned previously, Saudi Arabia is located in the most favorable region for incident solar radiation. This provides Saudi Arabia with a significant source of renewable energy. Saudi Arabia receives a daily average 6 kWh/m² or 13.5 TWh of solar energy [31]. This significant amount of solar radiation makes solar energy harvesting a profitable and sufficient renewable energy supply. Figure 3-3 shows the average horizontal solar irradiation for Saudi Arabia [32].

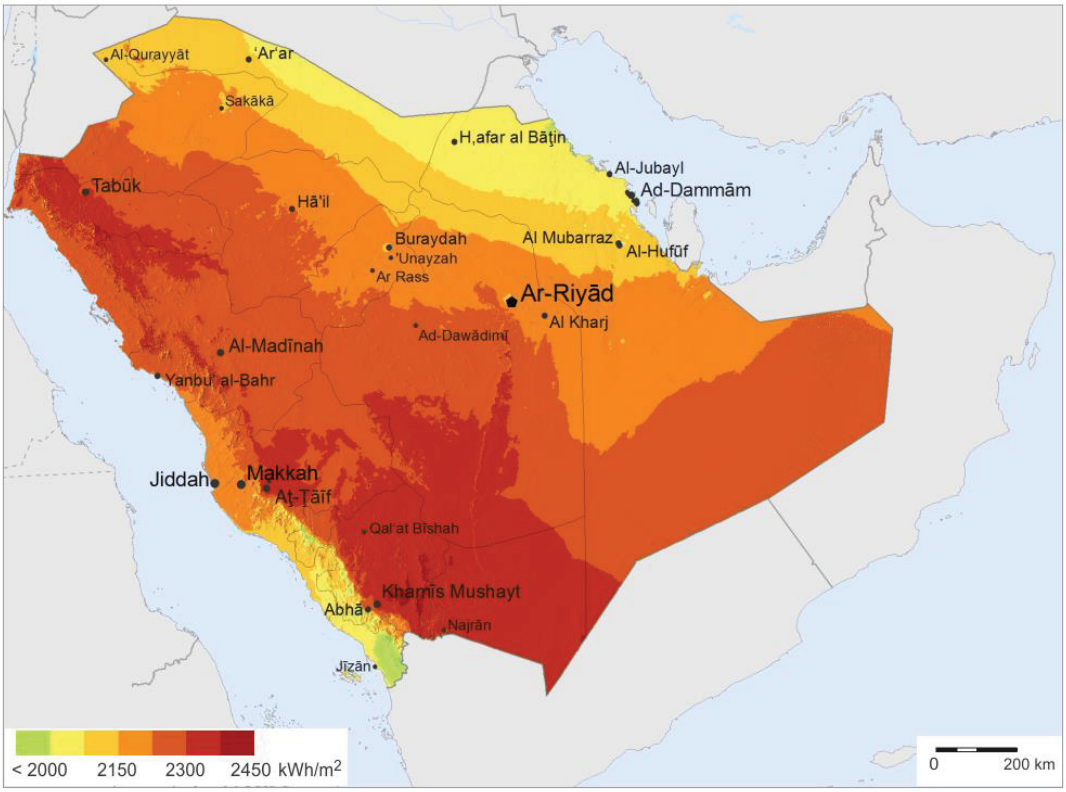

Figure 3-3 Global Solar Radiation in Saudi Arabia [32]

3.3.2 Solar Power in Saudi Arabia

The government of Saudi Arabia has had an interest in solar energy as an alternative energy source since the 1960's. In 1960 the Saudi Arabia government established the first PV beacon in Al-Madinah Al-Munnawara's airport [33]. In 1969 solar energy research began at the university level. In 1977 the Energy Research Institute (ERI) at King Abdulaziz City for Science and Technology (KACST) began working on solar energy technology. In the same year, the Saudi Arabian government launched the first joint venture in solar energy with the U.S. government, named *Solar Energy Research American-Saudi* (SOLERAS), which lasted until 1997 [34]. In 1980, SOLERAS provided two Saudi Arabian villages with solar power. From 1986 to 1991 the Saudi Arabian government instituted a cooperative program for research and development of solar-

hydrogen power (HYSOLAR) [35]. In 2010, the Saudi Arabian government developed the first solar powered water desalination plant. Recently, Saudi Aramco and King Abdullah University of Science and Technology (KAUST) installed solar power panels on the roof of the parking lot, which has a capacity of 2MW and 10MW respectively. In 2011 Saudi Arabia had the world's largest solar-thermal power plant, which used 36,305 square meters of solar panels to feed solar energy into a district-heating grid at Princess Nora Bint Abdul Rahman University in Riyadh. In 2012, King Abdullah Petroleum Studies and Research Center (KAPSARC) lunched a 3.5MW solar park in Riyadh [36].

In terms of solar radiation measurement, ERI started the Saudi Arabia Solar Radiation Atlas Project in cooperation with the National Research Energy Laboratory (NREL) in the United States in 1994. This project analyzed twelve various locations in Saudi Arabia. Global horizon irradiance (GHI), direct normal irradiance (DNI), diffuse horizontal irradiance, air temperature, and humidity data were collected. Also, NREL and KACST collaborated with NASA to validate satellite solar data. King Abdullah City for Atomic and Renewable Energy (KA.CARE) is the responsible agency overseeing Saudi Arabia's energy strategy [37].

Saudi Arabia is the 20th largest producer and consumer of electricity. It is facing issues with power generation due to population growth, a rapidly expanding industrial sector, and a high demand for air conditioning in the summer months. It is expected to increase the power capacity requirement to 120GW by 2020. This is almost double the current power capacity in Saudi Arabia [38]. Currently Saudi Arabia uses fossil fuels to generate power, however, by 2020 it is planned to have 55GW of renewable energy capacity, of which 41 GW will be from solar energy [30].

There are several obstacles involved with the development of the solar energy industry in Saudi Arabia. One of these obstacles is dust. In Saudi Arabia desert covers approximately 95% of the country [39]. Dust accumulation on PV cells in Riyadh reduces the efficiency by 32% within eight months [40]. Another obstacle is that the tariff on grid power from conventional sources is very cheap in comparison with solar energy power generation.

Chapter 4: Neural Networks

This chapter provides a brief overview of neural networks and how they can be applied to renewable energy generation.

4.1 Introduction

An artificial neural network (ANN) is a network that attempts to imitate brain functions. The human brain contains approximately 10^{11} neurons working in perfect harmony to perform a task. ANN's are designed to do a specific task through a learning process. By providing inputs and the desired output data, an ANN finds the relationship between the input and output data. Similar to a brain, where neurons are connected by synapses, the neurons in an ANN are connected by weighted inputs. Neurons are activated when the summation of these weighted inputs exceeds the neurons activation threshold [41].

There are seven successive steps involved in the design and implementation of an ANN [42]:

1. Collecting data
2. Creating the network
3. Configuring the network
4. Initializing the weights and biases
5. Training the network
6. Validating the network
7. Using the network

4.2 Artificial Neural Network Structure

ANN's consist of three parts: the input layer, neuron layer, and the output layer. Figure 4-1 shows a simple diagram of an ANN. The input vector x is multiplied by weight vector W. This multiplication of the input vector and weight vector, (Wx), is added to a bias, b, to form a net input, n. The net input, n, is then input to a neuron activation function to produce an output, a. The following equation defines the output of this neural network [42]:

$$a = f(W^T x + b) \tag{4.1}$$

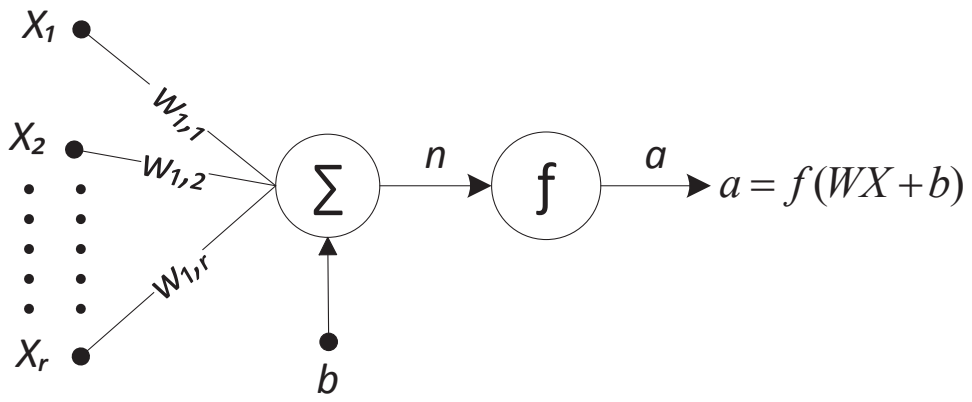

Figure 4-1 Single Neuron Network

Another important component in the ANN structure is the activation function. The activation function determines, depending on the summation of the weighted input *n*, if the neuron is activated or not. The activation functions can be divided into two categories, continuous or discrete. These functions can be unipolar or bipolar. Commonly used activation functions can be seen in Figure 4-2 [43].

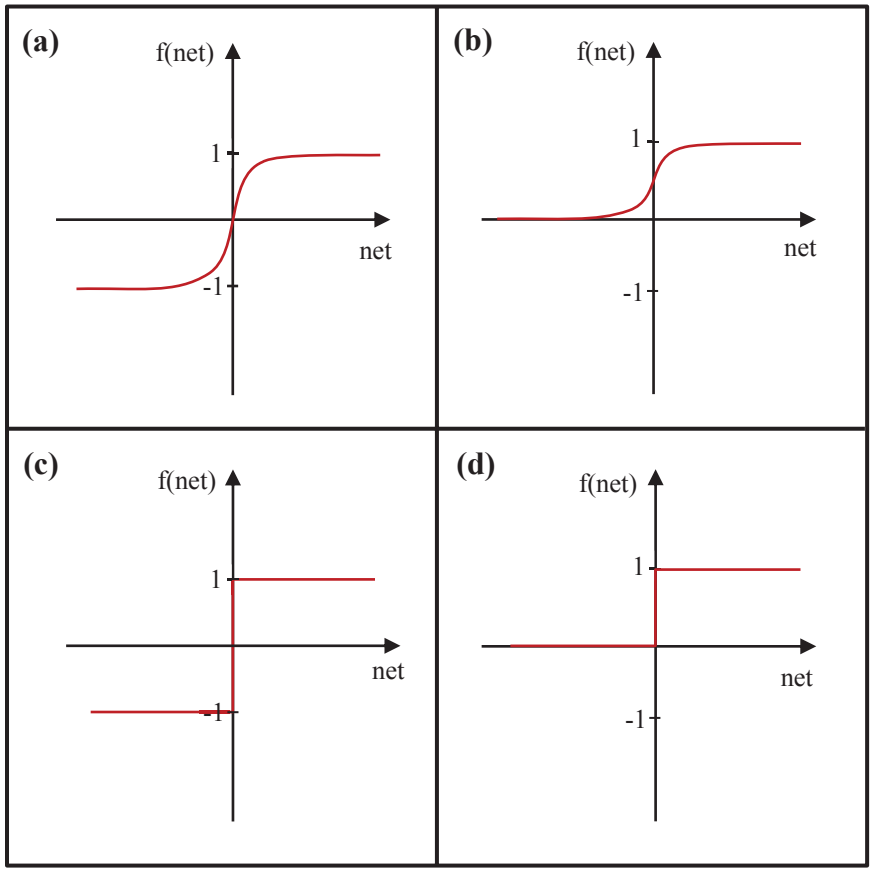

Figure 4-2 Commonly used activation functions: (a) Continuous Bipolar, (b) Continuous Unipolar, (c) Discrete Bipolar, (d) Discrete Unipolar

ANN can be divided into two main categories: single-layer and multi-layer, which will be explained in subsequent sections.

4.2.1 Single Layer Neural Network

Single-layer neural network (SLNN) is an extended case of the simple case mentioned in the previous section. SLNN consists of one layer of neurons as shown in Figure 4-3.

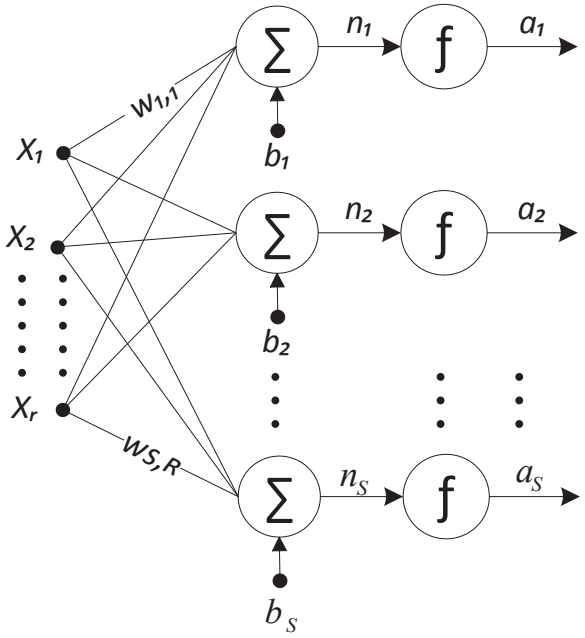

Figure 4-3 Single Layer Neural Network

Each input of the SLNN, x_i, is connected to all of the neurons in the layer by a weight vector, W. Every neuron adds its weight inputs ($W^T x$) and bias to form its net input, n_i. The net input vector n_i is used by the activation function, f, to form the neuron output vector a_i. The number of inputs is typically different than the number of neurons. The weight matrix, W, is given by:

$$\mathbf{W} = \begin{bmatrix} w_{1,1} & w_{1,2} & \dots & w_{1,R} \\ w_{2,1} & w_{2,2} & \dots & w_{2,R} \\ \\ w_{S,1} & w_{S,2} & \dots & w_{S,R} \end{bmatrix} \tag{4.2}$$

Where R is the number of elements in the input vector and S is the number of neurons [42].

4.2.2 Multi-layer Neural Network

Multi-layer neural networks (MLNN's) are used to implement complex problems that SLNN's are unable to solve. It has the ability to convert non-linearly-separable objects into a different domain where they become linearly separable. MLNN's include an input layer, output layer, and hidden layers as shown in Figure 4-4 [41].

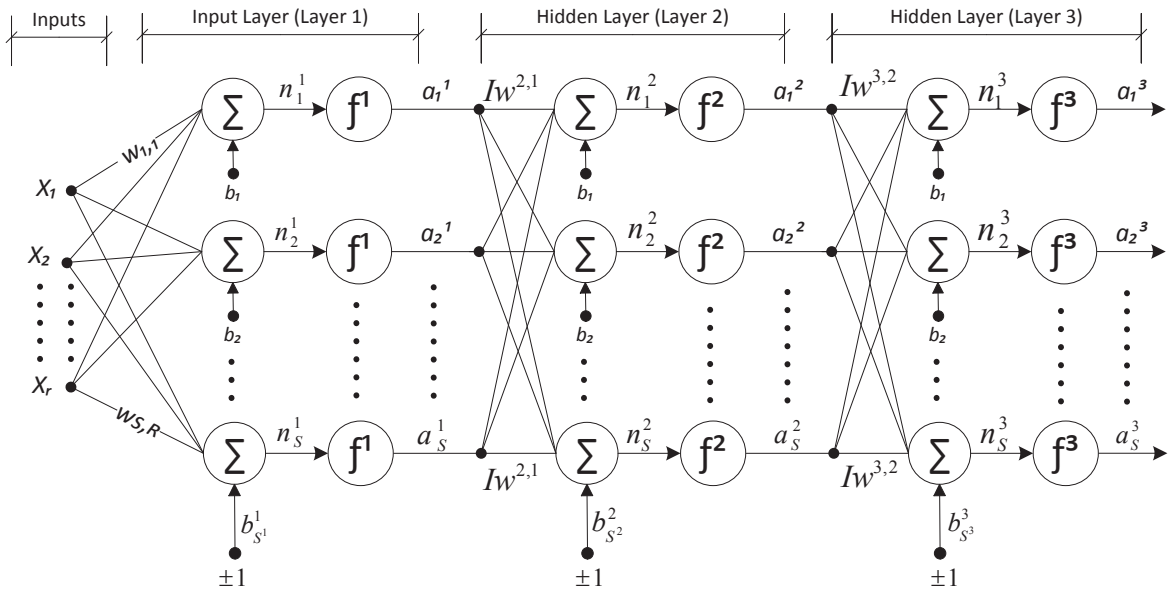

Figure 4-4 Multi-Layer Neural Network

In multi-layer networks the output of each layer becomes the input for the subsequent layer. Each layer has its own weight matrix. These weight matrices are varied to achieve a minimum total error. The output of a MLNN is given by [42]:

$$a^1 = f^1(IW^{1,1}X + b^1) \tag{4.3}$$

$$a^2 = f^2(IW^{2,1}a^1 + b^2) \tag{4.4}$$

$$a^3 = f^3(IW^{3,2}a^2 + b^3) \tag{4.5}$$

$$a^3 = f^3(LW^{3,2}f^2(IW^{2,1}f^1(IW^{1,1}X + b^1) + b^2) + b^3) \tag{4.6}$$

where,

X = input vector

IW = input weight matrix

LW = hidden weight matrix

b = bias vector

a = layer output vector

The hidden layer associated with multi-layer neural networks provides a powerful tool for performing very complex analysis.

4.3 Artificial Neural Network Phases

The data sets that are used in ANN's are divided into two main groups. The first group of data is used in the ANN training phase. This data covers almost two thirds of the total data set. In general the parameters of ANN's, weights and biases, will be modified in the training phase such that the ANN will model the data correctly [42].

In the training phase, there are two learning techniques, supervised and unsupervised. For the supervised learning technique, the ANN's parameters are initialized. The input data is introduced to ANN and generate the output of the first iteration. The output is compared to the desired value and the error between the two is calculated. Depending on the error's

value, the weights and biases are updated using different learning algorithms. This process is repeated until a minimum error is achieved. Using different learning algorithms such as Levenberg-Marquardt (LM), Bayesian Regularization (BR), and Resilient Back Propagation can produce neural networks with varying degrees of accuracy [43].

The two important learning algorithms are used in this work are LM and BR. LM is a technique that is used to find the minimum of a nonlinear least square function. The weights change can be calculated by this equation:

$$\Delta = -\frac{1}{2}\nabla E \tag{4.7}$$

where E is the mean-squared network error and can be found by:

$$E = \frac{1}{N}\sum_{k=1}^{N}[y(x_k) - d_k]^2 \tag{4.8}$$

where N is the number of examples, $y(x_k)$ is the network output corresponding to the example x_k, and d_k is the desired output for that example.

The algorithm starts with random weights. Based on Equation (4.7), the weights are updated by:

$$w_{t+1} = w_t + \Delta \tag{4.9}$$

The error is minimized every iteration until achieving the goal or a minimum is found. This is one of the fastest algorithms, and is highly recommended as a first-choice supervised algorithm. [42, 44]

The other learning algorithm used in this work is the Bayesian Regularization (BR) which is more advanced than standard back-propagation and can overcome its disadvantage of over-fitting. The Weight and bias values are updated by Levenberg-Marquardt optimization. BR finds the correct combination of squared errors and weights to produce a network that generalizes well. [42, 45]

The unsupervised technique is used when the desired output is unknown. Therefore, the weights and biases are updated based on the response to the inputs. Table 4-1 summarizes commonly used learning algorithms [41].

Table 4-1 Summary of Neural Network Learning Algorithms

Learning Rule	Weight Adjustment	Activation Function	Learning
Perceptron	$c[d_i - sgn({w_i}^t x)]x_j$ $j = 1,2,\dots,n$	Discrete	Supervised
Delta	$c(d_i - o_i)f'({w_i}^t x)x_j$ $j = 1,2,\dots,n$	Continuous	Supervised
Widrow-Hoff	$c(d_i - {w_i}^t x)x_j$ $j = 1,2,\dots,n$	Discrete or Continuous	Supervised
Outstar	$\beta(d_i - w_{ij})$ $i = 1,2,\dots,p$ For a layer of p neurons	Continuous	Supervised
Correlation	$cd_i x_j$ $j = 1,2,\dots,n$	Discrete or Continuous	Supervised
Hebbian	$co_i x_j$ $j = 1,2,\dots,n$	Discrete or Continuous	Unsupervised
Winner-take-all	$\alpha(x_j - w_{mj})$ $j = 1,2,\dots,n$ m is the winning neuron	Continuous	Unsupervised

After the training phase, the second group of data is introduced for checking the ANN model validity.

4.4 Literature Review

There are many limitations to using PV technology. Solar energy is intermittent and variable, resulting in power fluctuations which require precise prediction techniques. Many methods have been proposed to overcome these challenges such as artificial intelligence (AI) techniques, which include expert systems (ES), artificial neural networks (ANN), genetic algorithms (GA), fuzzy logic (FL), and many hybrid systems [46, 47].

ANN is the most common AI technique that has been used for the last two decades. It can model complex and nonlinear systems because of the network's ability to adjust its weights and biases. There are many ANN structures, such as, the multilayer perceptron (MLP), recurrent neural network (RNN) and radial basis function network (RBF) [41]. These various structures make ANN's very versatile in their applications. ANN's can be used to predict solar radiation, which helps the management of power generated from a PV system [46, 47].

Numerous meteorological and geographical variables such as maximum temperature, relative humidity, sunshine duration, cloud cover, latitude, longitude, and altitude have been used to develop ANN models for solar prediction [48].

Significant research has been conducted regarding solar energy forecasting using ANN techniques. Sozen et al. (2004) [49] used latitude, longitude, altitude, months, mean sunshine duration, and mean temperature as inputs to an ANN model to predict the solar

potential in Turkey. In this model, a data set covering three years (2000-2003) and 17 locations was used for training and testing. Various combinations of layers and neurons were used as well as three different learning algorithms. The maximum mean absolute percentage error was used to validate the model. The error was approximately 6.74% and the absolute fraction of variance, R^2, values were 99.89% for the testing stations.

Tymvios et al. (2005) [50] used the same input variables as Sozen et al. (2004) [49] to train seven ANN models to estimate the solar radiation on a horizontal surface. They used the back propagation feed forward method with tangent sigmoid as an activation function. The ANN models vary between one and two hidden layers and the number of neurons between 23 and 77. The model with two hidden layers and 23 and 46 neurons respectively was found to be the best. The mean biased error (MBE) and root mean square error (RMSE) values were 0.12% and 5.67%, respectively. This study was based on seven years worth of data (1986-1992) collected at Athalassa, Cyprus.

Rehman et al. (2008) [51] used three combinations of data sets to estimate the global solar radiation (GSR) in Abha, Saudi Arabia. In this model, a data set of four years (1998-2001) had been used as training data and one year time span (2002) as testing data. The input combinations were: (i) day of the year and daily maximum air temperature, (ii) day of the year and daily mean air temperature (iii) day of the year, daily mean air temperature, and relative humidity. By using back propagation and a multilayered feed forward ANN with 24, 32 and 24 neurons for the three combinations respectively, the absolute mean percentage errors were 10.3%, 11.8% and 4.49, respectively.

Mubiru et al. (2008) [48] used latitude, longitude, altitude, sunshine hours, cloud cover, and maximum temperature data as inputs to an ANN model. The model was used to estimate the monthly average daily global solar radiation in Uganda. In this model, a three year time span of data (April 2003-December 2005) had been used. Various training algorithms and number of neurons was investigated. It was found that the best model was with 15 neurons and one hidden layer using the Levenberg–Marquardt training algorithm. This model showed $R^2$and RMSE of 0.974 and 38.5% respectively.

Zervas et al. (2008) [52] used weather conditions (cloud, rain or clear day) and each calendar day data as inputs to the ANN model to predict the daily global solar irradiance (GSI) distribution on horizontal surfaces at a particular location in Greece. In this model, radial basis function (RBF) ANN was used. This paper showed a coefficient of determination R^2 of over 0.98.

Moustris et al. (2008) [53] used latitude, longitude, altitude, sunshine hours, cloud cover, hourly data of air temperature, and relative humidity data as inputs to the ANN model. This model was used to create hourly global and diffuse solar irradiance data at seven locations in Greece. When training the ANN the data was divided into two sets: warm and cold seasons. This created an absolute maximum, average, and absolute minimum data of global and diffuse solar irradiance for each month. In this work, multilayer perceptron (MLP) ANN with a back propagation learning algorithm was used. The average correlation coefficient was found to be about 0.99, 0.98 and 0.7 for maximum, average, and minimum hourly global and diffuse solar irradiance respectively.

Lam et al. (2008) [54] used latitude, longitude, altitude, day number, daily mean temperature, and sunshine hours as input data to the ANN model. This model was used to predict the daily global solar radiation for 40 different locations in China. The ANN model used was multi-layered with a back propagation training algorithm. The results showed that the coefficients of determination, R^2, decreased from colder to warmer climates. Moreover, there was a strong correlation between daily solar radiation and the corresponding sunshine hours. The RMSE varied from 9.1% in severe cold climates to 20.5% in cold climates.

Alam et al. (2009) [55] used different combinations of latitude, longitude, altitude, time, months of the year, air temperature, relative humidity, rainfall, wind speed, and net long wavelength data as inputs to ANN models. The models were used to estimate the monthly mean hourly and daily diffuse solar radiation for 10 different Indian stations. The proposed models used three layers of feed forward with back propagation algorithm. The high coefficient of determination R^2 (higher than 0.85) indicated a strong correlation between the diffuse solar radiation and the input variables. The RMSE for hourly diffuse solar radiation and monthly mean daily diffuse solar radiation varied between 1.1% and 8.8% and between 1.3% and 4.5% respectively.

Ghanbrazadeh et al. (2009) [56] have used different combinations of air temperature, relative humidity, and sunshine hour values as inputs to ANN models. The model was used to predict daily global solar radiation (GSR) for Dezful City in Iran. In this model, data over a four-year time span (2002-2005) was used for training the networks while 235 days of data was used for testing it. Three feed forward back propagation ANN models were used with three hidden layers. Three neurons were used in the first layer and two or

three neurons in the second layer. The outperforming model was then used all the three variables as inputs. For this model, the absolute mean percentage of error was 8.84%.

Mellit et al. (2010) [57] used huorly solar irradiance, hourly air temperature, and hours of the day as inputs to an ANN model. This model was used in forecasting 24 h ahead of solar irradiance at Trieste in Italy. The proposed model used multilayer perceptron MLP feed forward with the back propagation-training algorithm. The model had four layers with 3, 11, 17, and 24 neurons respectively. In this model, the correlation coefficient and RMSE were in the range of 98–99% and 13-67% respectively for sunny days while in the range of 94–96% and 54-85% respectively for cloudy days.

Deng et al. (2010) [58] used twelve different combinations of latitude, longitude, altitude, sunshine duration, air temperature, rainfall, relative humidity, atmospheric pressure, and day of year as input data to ANN models. This model was used to estimate the daily global solar radiation at ten different locations in China. Eight-years of data was used to train and test the model. The proposed ANN models used three layers of feed forward neural network with back propagation training algorithm. In these models, the first and second layers had between 4-9 and 6-25 neurons respectively, while the third layer -the output layer- had only one neuron. This paper concluded that the most significant variable was sunshine duration. In this study, it was found that the best model was the one that used all input variables. The best model was found when all input variables were used. The model, RMSE and correlation of determination, R^2, were 1.915 MJ/m^2 and 0.932 respectively.

Wang et al. (2011) [59] used diffused radiation, temperature, relative humidity, and time, as inputs to ANN models. The model was used for short-term solar irradiation prediction in Golden, CO, USA. These models used multilayered feed forward neural network with backward propagation (BP) training algorithm. Among different combinations of ANN layers and neurons, the best model had four layers with 24, 18, 13 and 24 neurons respectively. The RMSE and the correlation of determination, R^2, were 0.0331 and 0.9912 respectively.

Angela et al. (2011) [60] have used only one variable, sunshine duration as an input to the ANN model. The model was used to estimate the monthly average daily global solar irradiation on a horizontal surface at Kampala, Uganda. Five years of data (2003-2008) was used for training and testing the models. All models tested in this paper used feed forward back propagation neural networks. Among dozens of models using different numbers of neurons, the proposed model had one hidden layer with 65 neurons. It had a RMSE and a correlation coefficient of 0.521 and 0.963 respectively.

Rani et al. (2012) [61] used six different combinations of temperature, humidity, date, and month of the year as input to an ANN model. This model was used to predict the daily GSR under clear sky conditions of any location in India. Three years of data (2000-2002) were used to train and test the back propagation feed forward neural network model. This model had three layers with 10 neurons in the hidden layer. The authors concluded that using all the above variables led to a better estimation of radiation MAPE as 9.1754% and RMSE as 0.9429.

Alharbi, M. (2013) [62] used different combinations of temperature, humidity, and daily date code as inputs to ANN models. The model was used to predict the daily global solar radiation for a specific location in Riyadh, Saudi Arabia. Three years of data (2009-2011) were used to train and test the models. The models consisted of three layers with the number of layer neurons varying from 60 to 83 in the hidden layer. These models used the back propagation learning technique. This study concluded that the best prediction was when all of the three inputs were used. The best model had 80 neurons in the hidden layer. The RMSE and the Correlation Coefficient were 7.5% and 0.986 respectively.

Chapter 5: Modeling, Simulation and Discussion

This chapter presents a Global Solar Radiation (GSR) prediction model. The simulation results of this model are obtained by using MATLAB™ and artificial neural network (ANN) modelling.

The modeling and analysis were divided in general into three main steps as shown in Figure 5-1. In the first step, all weather variables were examined to determine which variables provide the best GSR prediction. The second step constructs the proposed GSR model by using the weather variables that were chosen in the first step. Finally, the proposed model was compared with other works that have been conducted in this field.

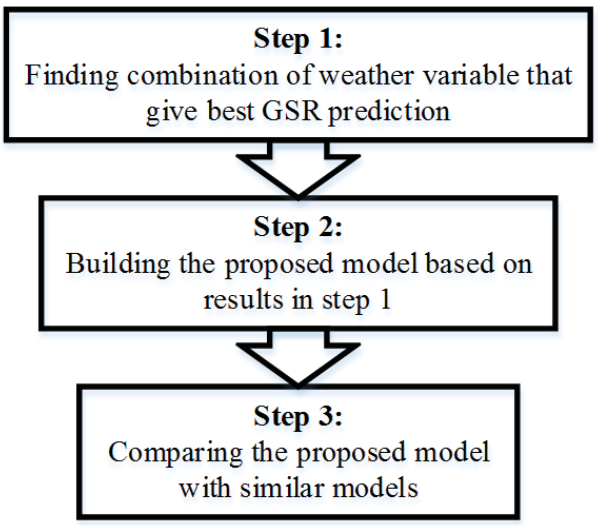

Figure 5-1 Flow Chart of GSR Prediction

In this work, air temperature, relative humidity, pressure, cloud-cover, vapor, wind-speed and direction, and the day, were used as data inputs for the GSR prediction model. This data was collected from Solar Village in Riyadh, Saudi Arabia between 2007 and 2010.

5.1 Effect of Weather Variables on GSR Prediction

The first step, for model constricting, was to determine the effect of each variable on the GSR predictions. Each variable was taken individually with the day as inputs for the neural network model to predict the daily average GSR as shown in Figure 2-1. In this model, three layers - input, hidden and output- with different combinations of transfer functions have been used.

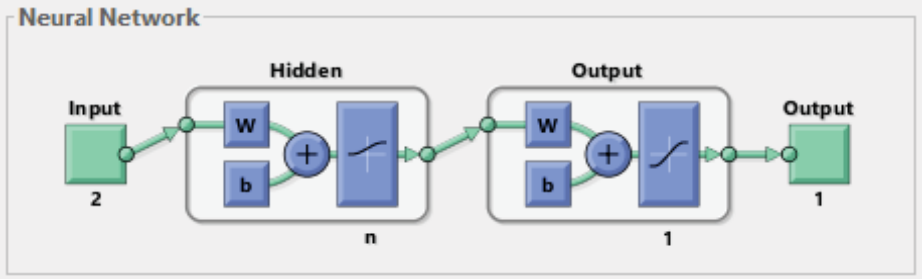

Figure 5-2 Structure of Model ANN-1

Among sets of different combinations of transfer functions, logsig and tansig were found to be the best combination candidates. Logsig and tansig were used for the hidden and output layers respectively. Furthermore, the number of neurons was chosen to provide small values of Root Mean Square Error (RMSE) and Mean Absolute Percentage of Error (MAPE) as well as a large value of correlation coefficient (r) as shown in Table 5-1.

RMSE was used to explain the model's fit and the difference between actual and predicted data. MAPE was calculated to find the absolute average error between the actual and predicted values. Finally, r showed how strongly the relation between the measured and predicted value was. These values were given by [63]:

$$RMSE = \sqrt{\frac{1}{N}\sum_{1}^{N}(y_i - t_i)^2} \tag{5.1}$$

$$MAPE = \frac{1}{N}\sum_{1}^{N}\left|\frac{y_i - t_i}{t_i}\right| \tag{5.2}$$

$$r = \frac{n(\sum y_i t_i) - (\sum t_i)(\sum y_i)}{\sqrt{(n\sum {y_i}^2 - (\sum y_i)^2)(n\sum {t_i}^2 - (\sum t_i)^2)}} \tag{5.3}$$

where, y is the predicted value, t is the actual value and N is the number of observations.

Table 5-1 Performance Evaluation of Average Daily GSR Prediction with One Weather Variable plus the Day

Model	**Input**	**Output**	**Neuron**	**RMSE**(%)	**MAPE**(%)	**r**
ANN_1.1	d, cc	GSR_{avg}	80	7.1956	4.3578	0.96497
ANN_1.2	d, H	GSR_{avg}	140	10.348	5.0602	0.95016
ANN_1.3	d, T	GSR_{avg}	131	11.916	6.0378	0.94944
ANN_1.4	d, V	GSR_{avg}	85	15.403	7.7645	0.93754
ANN_1.5	d, P	GSR_{avg}	160	23.172	7.9816	0.92044
ANN_1.6	d, w_d	GSR_{avg}	185	25.179	8.3467	0.90182
ANN_1.7	d, w_s	GSR_{avg}	159	27.340	8.1628	0.90840

From Table 5-1, temperature, humidity and cloud-cover resulted in lower RMSE and MAPE and higher r when they were used individually with the day to predict the daily average GSR. This means that these input variables play an important role in the GSR prediction process.

In the second step, two weather variables with the day were used as inputs for the daily average GSR prediction as shown in Figure 5-3. Table 5-2 shows the best combinations of inputs that resulted in lower RMSE and MAPE and higher r.

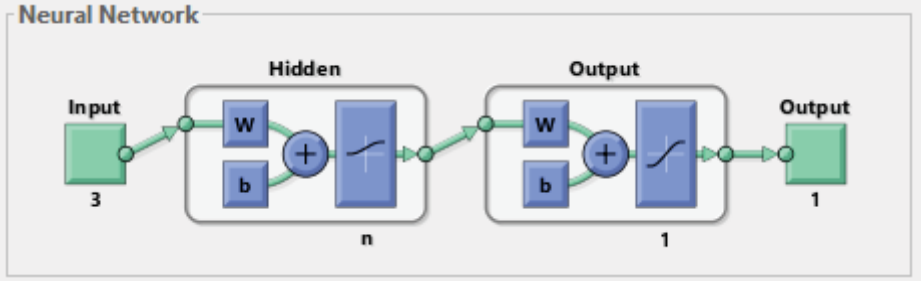

Figure 5-3 Structure of Model ANN-2

Table 5-2 Performance Evaluation of Average Daily GSR Prediction with Two Weather Variables plus the Day

Model	Input	Output	Neuron	RMSE(%)	MAPE(%)	r
ANN_2.1	d, H, cc	GSR_{avg}	159	4.0337	3.1476	0.98711
ANN_2.2	d, T, cc	GSR_{avg}	178	4.3336	3.4697	0.98520
ANN_2.3	d, T, H	GSR_{avg}	75	4.7531	3.6568	0.98025
ANN_2.4	d, cc, V	GSR_{avg}	115	5.1004	3.9068	0.98013

Comparing Table 5-2 with Table 5-1, using humidity and cloud-cover, temperature and cloud-cover or humidity and temperature as inputs provided better prediction than using only one variable with the day.

Next, more than two weather variables with the day were used as inputs for daily average GSR prediction as shown in Figure 5-4. Table 5-3 shows the best combination of inputs that provide lower RMSE and MAPE and higher r.

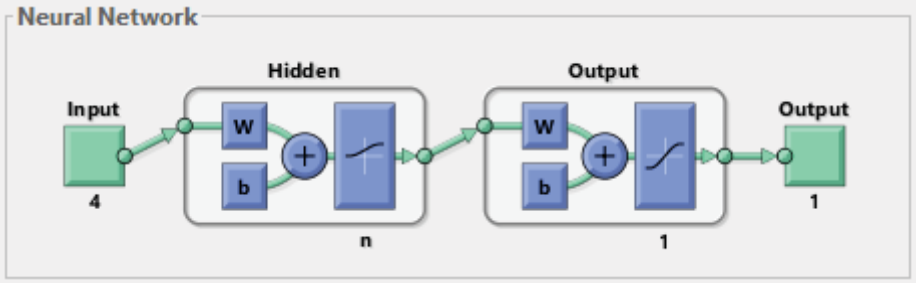

Figure 5-4 Structure of Model ANN-3

Table 5-3 Performance Evaluation of Average Daily GSR Prediction with More Than Two Weather Variables plus the Day

Model	Input	Output	Neuron	RMSE(%)	MAPE(%)	r
ANN_3.1	d, T, H, cc, V	GSR_{avg}	160	3.4764	2.2557	0.99202
ANN_3.2	d, T, H, cc	GSR_{avg}	65	3.8191	2.951	0.98905

Table 5-3 shows a very good result when temperature, humidity, cloud-cover and the day were used to predict the daily average GSR. Also, adding vapor as an input enhanced the prediction process. Comparing Table 5-3 with Table 5-1 and Table 5-2 shows that using more input weather variables increases the prediction accuracy. However, the values of $RMSE$, $MAPE$ and r from Table 5-3 are slightly better than the values in Table 5-2 and much better than the values in Table 5-1. Therefore, the proposed model used only two weather variables with the day to achieve a simple model with the best prediction.

Cloud-cover, humidity and temperature are the best candidates for GSR prediction. Cloud-cover has the best effect on GSR prediction; cloud-cover was excluded because it is difficult to be predicted. However, when the cloud-cover data is available, it can be used in ANN-2.1 and ANN-2.2 models for better GSR prediction. Therefore, in this

thesis, the proposed model used air temperature, humidity and the day as inputs for GSR prediction.

5.2 GSR Prediction Modeling

The proposed model consists of many sub-models as shown in Figure 5-5. In the first sub-model, the average temperature and humidity and the day were used as inputs for GSR prediction. In the second sub-model, air temperature was predicted by using previous temperature, GSR and humidity data with the day as input. The third sub-model predicted humidity by using previous temperature, GSR and humidity data with the day as input. The last sub-model used the predicted temperature and humidity from the second and the third sub-models for GSR prediction.

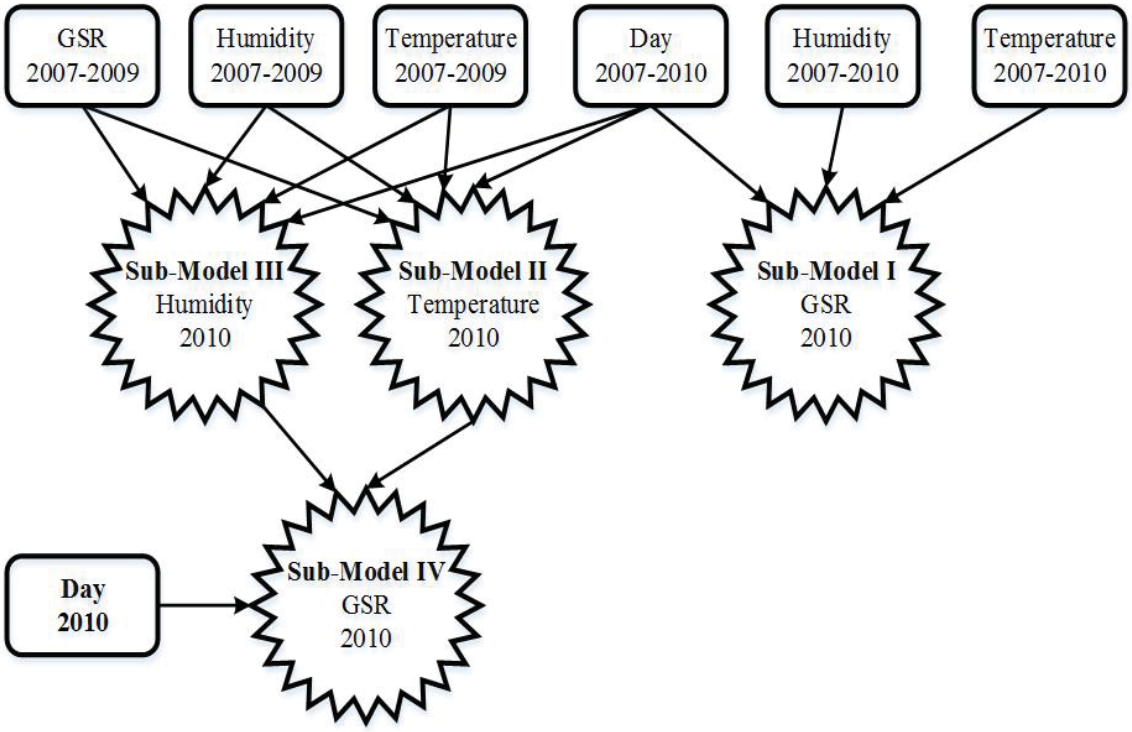

Figure 5-5 General Structure of the Proposed Model

5.2.1 Sub-Model I: Predicting GSR Using Actual Weather Variables

In this model, the average daily GSR for 2010 was predicted by using the daily average of temperature and humidity, and the day as inputs from 2007 to 2010. This model used feed forward ANN and was divided into three layers as shown in Figure 5-6. The hidden layer has $logsig$ as a transfer function while the output layer has $tansig$. The input data was divided into three sets: 70% of the data for the training phase, 15% of the data for the validation phase and 15% of the data for the testing phase. Using the BR algorithm in the training phase with 75 neurons in the hidden layer and one neuron in the output layer gave the best average GSR prediction.

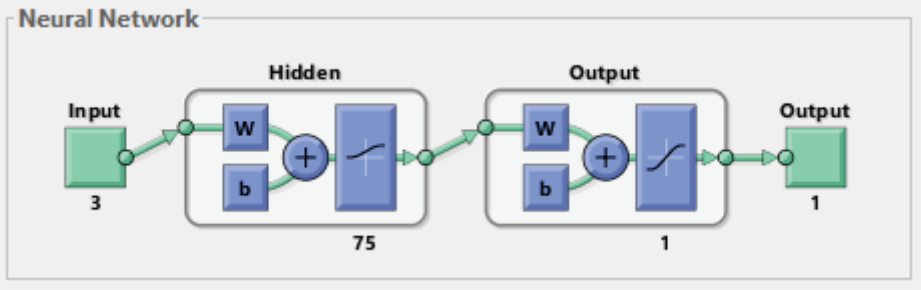

Figure 5-6 Daily Average GSR Model Structure

The $RMSE$, $MAPE$ and r for this model are shown in Table 5-4. From this table, the small value of RMSE indicates the small error between the actual and predicted GSR values. The high value of r shows how decent the fit is between the actual and predicted GSR values. In addition, the model has a small number of neurons which makes the model less complicated. Figure **5-7** shows the similarity between the predicted and actual GSR data. Figure 5-8 shows the fit between the predicted and actual data.

Table 5-4 Performance Evaluation of Average Daily GSR Prediction for Sub-Model I

Model	Input	Output	Neuron	RMSE(%)	MAPE(%)	r	Training time (s)
Sub-Model I	d, T, H	GSR_{avg}	75	4.7531	3.6568	0.98025	14.58

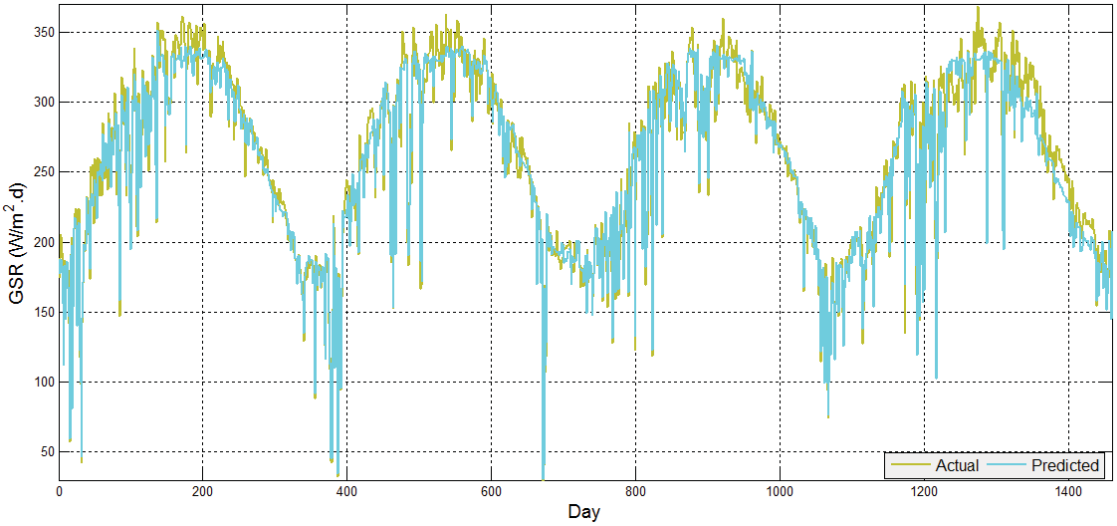

Figure 5-7 Actual and Predicted Daily Average GSR Values from 2007 to 2010

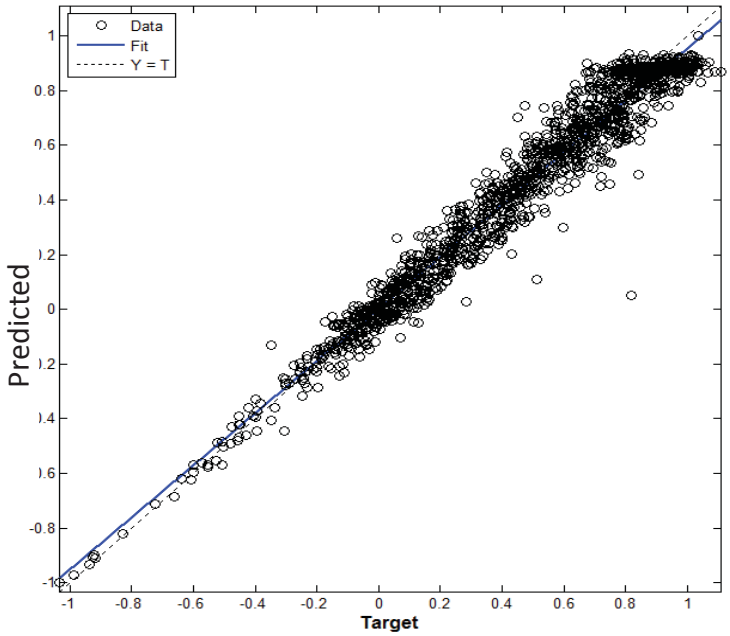

Figure 5-8 The Fit between Act Actual redicted Daily Average GSR

5.2.2 Sub-Model II: Predicting the Daily Average Air Temperature

This model predicts the daily average temperature for 2010. This model is needed when there is a lack of temperature data. This model used average GSR, temperature and humidity data for 2007 to 2009 and the day as inputs. These inputs were divided into three sets: 70%, 15% and 15% for training, validation and testing phase respectively. These inputs were introduced into a three layers feed forward ANN with $logsig$ and $tribas$ transfer function in hidden and output layer respectively as shown in Figure **5-9**. The best result achieved was when BR algorithm was used with 151 neurons in the hidden layer and one neuron in the output layer.

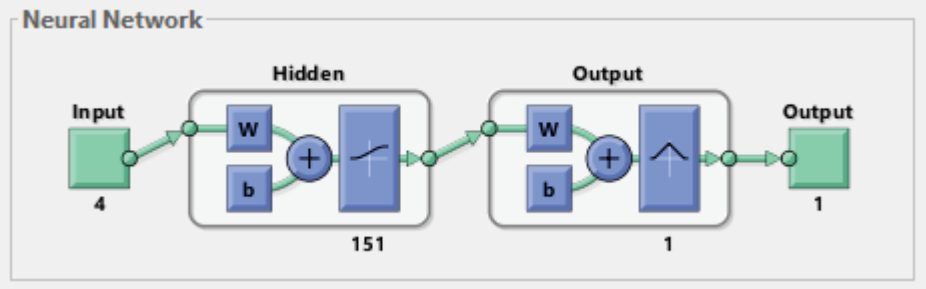

Figure 5-9 Daily Average Temperature Model Structure

Table 5-5 shows the $RMSE$, $MAPE$ and r for this model. From this table, the $RMSE$ value is 10.7% which is considered a good performance. Also, r value is 0.963 which indicates a good fit between the actual and predicted temperatures. Furthermore, this model has four inputs and a relatively small number of neurons making the model fairly simple. The actual and predicted average daily temperature values are shown in Figure **5-10** while Figure **5-11** shows the fit between the predicted and actual data.

Table 5-5 Performance Evaluation of Average Daily Temperature Prediction for Sub-Model II

Model	Input	Output	Neuron	RMSE(%)	MAPE(%)	r
Sub-Model II	d, T, H, r	t	151	10.715	6.3407	0.96259

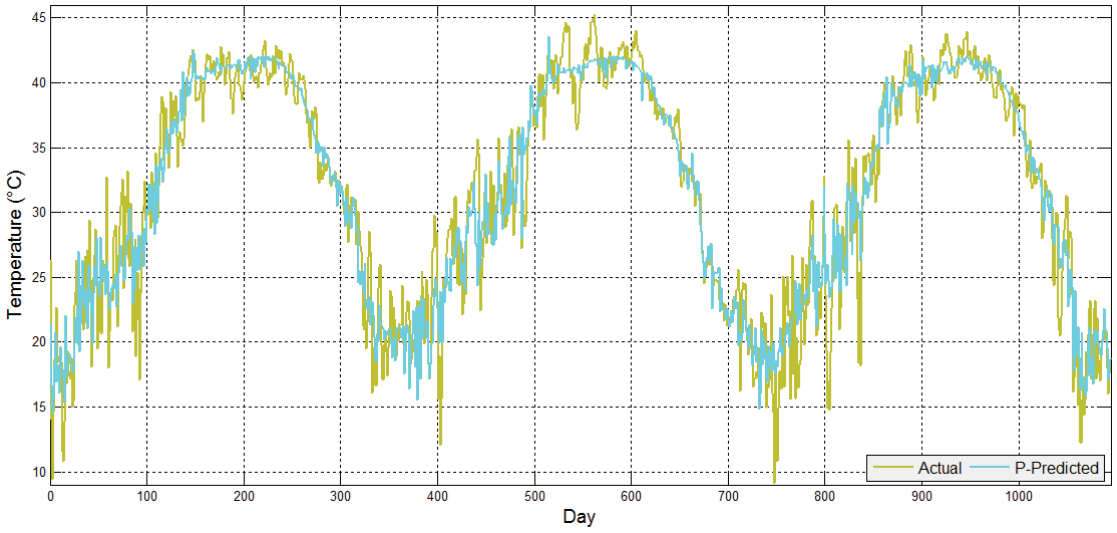

Figure 5-10 Actual and Predicted Daily Average Temperature Values from 2008 to 2010

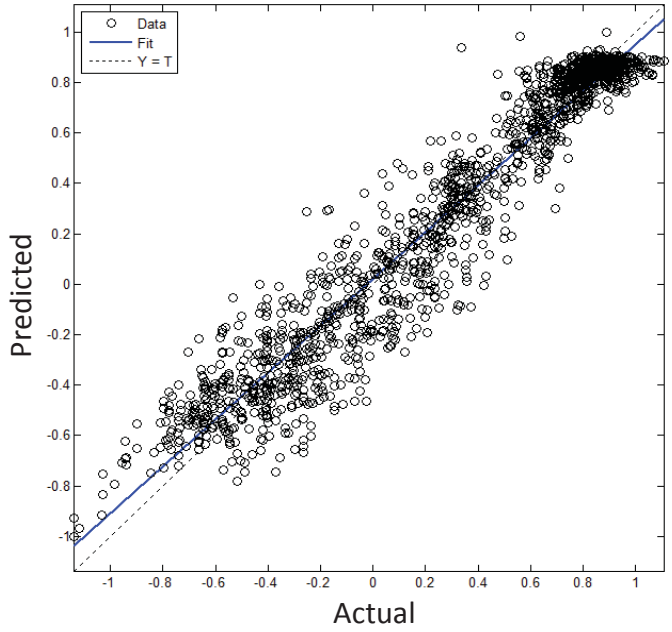

Figure 5-11 The Fit between Actual and Predicted Daily Average Temperature

5.2.3 Sub-Model III: Predicting the Daily Average Relative Humidity

This model predicts the daily average humidity for 2010. As the previous model, this is a necessary model when humidity data is unavailable. Average GSR, temperature and humidity data for 2007 to 2009 and the day were used as inputs. The data were divided 70% for training, 15% for validation and 15% for testing purpose. The model used feed forward ANN and three layers. The transfer functions in hidden and output layers were $logsig$ and $tansig$. Figure **5-12** shows the model structure. By using LM algorithm, the best number of neurons found was 135 in the hidden layer and one neuron in the output layer.

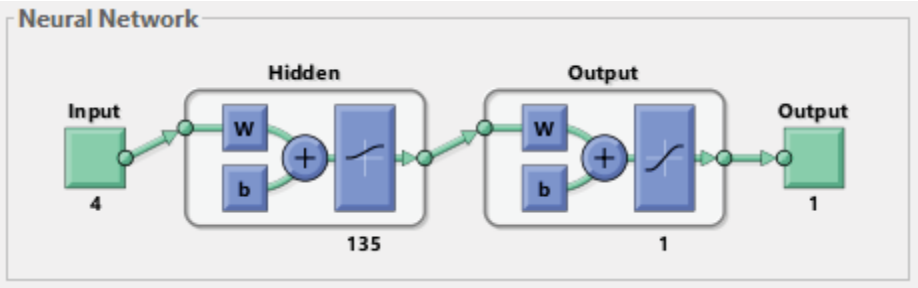

Figure 5-12 Daily Average Humidity Model Structure

The prediction of humidity is not easy to discern, because of its high fluctuation. Table 5-6 shows the performance evaluation of this model. The RMSE and MAPE are 0.15 and 9.06 respectively. Also, the fit between the actual and predicted humidity is 0.94 which is considered a good fit. Figure **5-13** shows the similarity between the predicted and actual humidity data. Figure **5-14** shows the fit between the predicted and actual data.

Table 5-6 Performance Evaluation of Average Daily Humidity Prediction for Sub-Model III

Model	Input	Output	Neuron	RMSE(%)	MAPE(%)	r
Sub-Model III	d, T, H, r	H	135	15.009	9.0621	0.94436

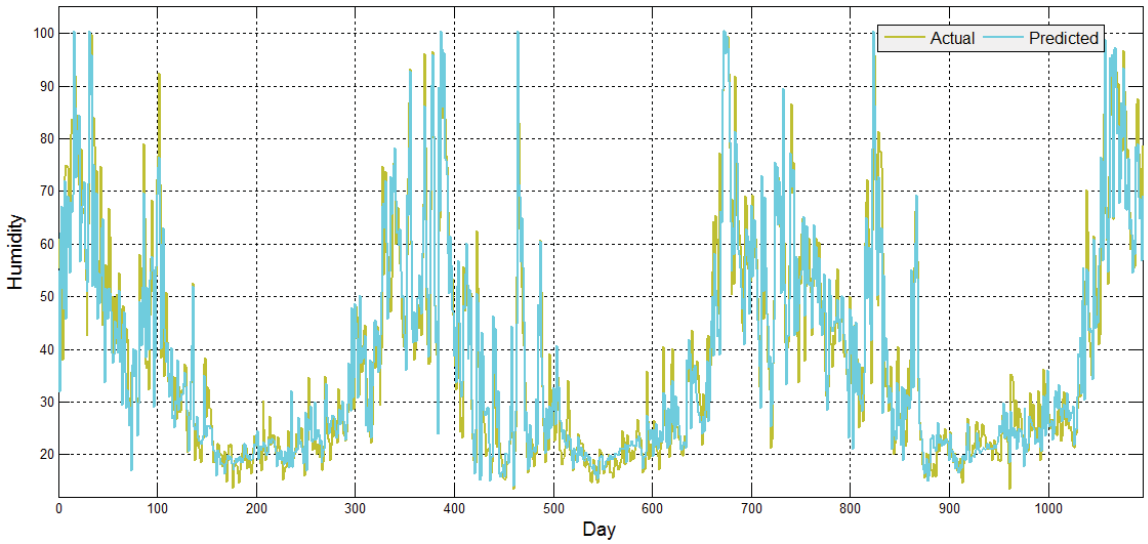

Figure 5-13 Actual and Predicted Daily Average Humidity Values from 2008 to 2010

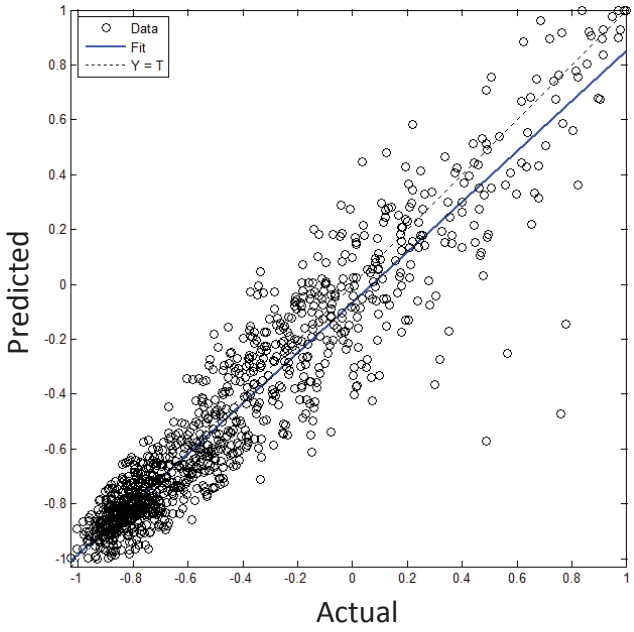

Figure 5-14 The Fit between Actual and Predicted Daily Average Humidity

5.2.4 Sub-Model IV: Predicting GSR Using Predicted Weather Variables

This is an alternative model used when one or more of the input variables were predicted by sub-model II or III. This model predicted the average GSR in 2010 by using the model II and III outputs and the day of 2010. The input data were divided into three sets: 70%, 15% and 15% for training, validation and testing phase respectively. The model has three layers. The transfer functions for hidden and output layer were *logsig* and *tansig* respectively. With BR algorithm and 115 neurons in the hidden layer and one neuron in the output layer, the model achieved the best prediction.

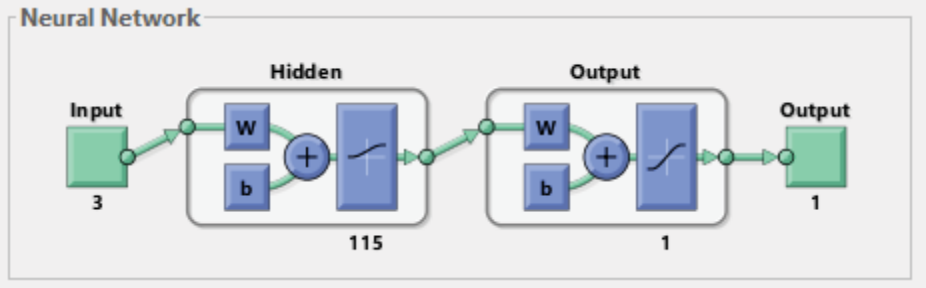

Figure 5-15 Daily Average GSR Model Structure

Table 5-7 shows the RMSE, MAPE and r for this model. The values of RMSE, MAPE and *r* are 0.07, 6.09 and 0.94 respectively. Figure **5-16** shows the similarity between the predicted and actual GSR data. Figure **5-17** shows the fit between the predicted and actual data.

Table 5-7 Performance Evaluation of Average Daily GSR Prediction for Sub-Model IV

Model	**Input**	**Output**	**Neuron**	**RMSE**(%)	**MAPE**(%)	**r**
Sub-Model IV	d, T, H	GSR_{avg}	115	7.1492	6.0868	0.93887

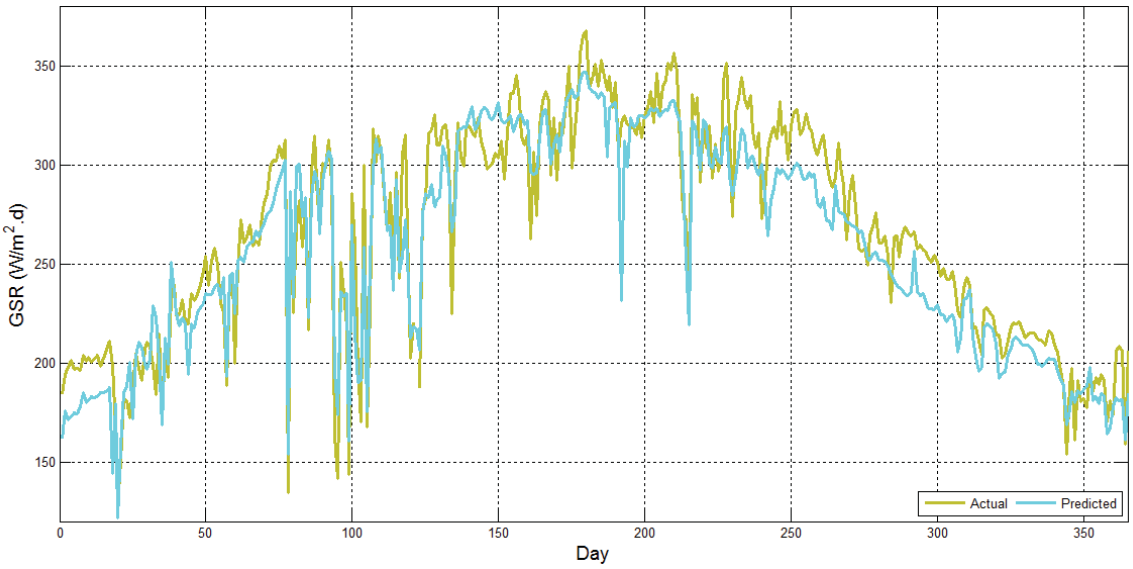

Figure 5-16 Actual and Predicted Daily Average GSR Values from 2007 to 2010

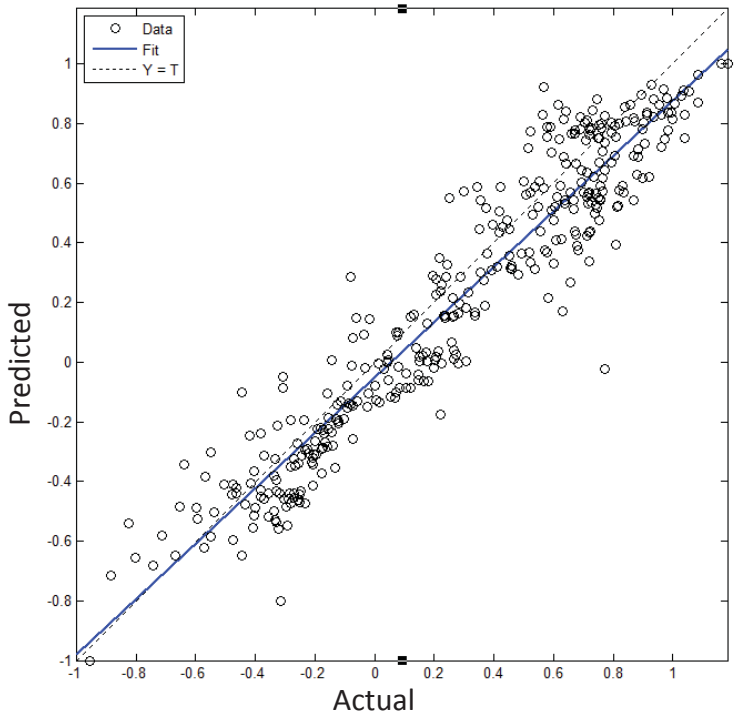

Figure 5-17 The Fit between Actual and Predicted Daily Average GSR

5.3 Effect of changing the number of neurons on RMSE, MAPE and r

The highest number of neurons does not improve the accuracy of GSR predictions for forecasting. Figure A-1 through to Figure **A-7** plot the RMSE (%), MAPE (%) and r versus the number of neurons. These show that increasing the number of neurons did not necessarily mean greater accuracy and better results in GSR predictions regardless of the combination of weather variables. Indeed, Figure A-1 shows the optimal number of neurons for predicting daily GSR when cloud cover is the variable to be 80, Figure **A-2** shows the optimal number of neurons for predicting daily GSR when humidity is the variable to be 140, Figure **A-3** shows the optimal number of neurons for predicting daily GSR when temperature is the variable to be around 130, Figure **A-4** shows the optimal number of neurons for predicting daily GSR when vapor is the variable to be 85, Figure **A-5** shows the optimal number of neurons for predicting daily GSR when pressure is the variable to be between 160, Figure **A-6** shows the optimal number of neurons for predicting daily GSR when wind direction is the variable to be between 185 and Figure **A-7** shows the optimal number of neurons for predicting daily GSR when wind speed is the variable to be around 160.

Similar trends, where increase in number of neurons does not necessarily mean greater accuracy in GSR prediction as measured by r, MAPE and RMSE are seen in Figure **B-1** through to Figure **D-4** where combinations of weather variables are included in the modelling.

5.4 Comparison with other Approaches

It is noted that because each author presents specific to different geographic locations and weather conditions, comparisons are given for illustration purposes. Table 5-8 presents the result of the proposed model and other works conducted in GSR prediction, including an overview of the important variables, structural complexity and performance of different models. Note that Mellit et al results are not valid for GSR forecasting.

Table 5-8 Comparative study between the developed model and other GSR ANN-models

Inputs	Layers	Neurons	RMSE(%)	MAPE(%)	r(%)	Author
$\mathbf{S_m, S_t, T_m}$	4	69	5.67	-	-	Tymvios et al. (2005)
$\mathbf{S_m, S_t, T_m}$	3	46	5.97	-	-	Tymvios et al. (2005)
d, T	3	32	-	11.80	-	Rehman et al. (2008)
d, T, H	3	24	-	4.49	-	Rehman et al. (2008)
T, r	4	55	13.14	-	99	Mellit et al. (2010)
G,t,H,h	4	79	4.50	0.60	96.4	Wang et al. (2011)
$\mathbf{S_m}$	3	65	52	1.97	96.3	Angela et al. (2011)
T	3	10	-	12.62		Rani et al. (2012)
H	3	10	-	13.52		Rani et al. (2012)
d, M	3	10	-	10.52		Rani et al. (2012)
T, H, d, M	3	10	-	9.18		Rani et al. (2012)
d	3	83	18.53	8.14	86.2	Alharbi, M (2013)
d, T, H	3	83	7.91	1.82	98.2	Alharbi, M (2013)
d, T, H	3	75	4.75	3.66	98.02	Proposed model

The proposed model has better results in terms of RMSE value in comparison with other models proposed in the literature. However, Wang et al. (2011) has lower RMSE value, but with more complicated structure. Furthermore, comparing the model structure with other models that have three inputs, the proposed model has less number of neurons compare to Alharbi, M (2013). However, Rehman et al. (2008) and Tymvios et al. (2005)

models have fewer neurons, but higher RMSE. Rani et al. (2012) and Rehman et al. (2008) have different models with simpler structures, but, with higher MAPE.

Chapter 6: Conclusions and Future work

This chapter summarizes the results of this thesis and the contributions that were made. Suggestions for future work are also discussed.

6.1 Conclusions

A new model for predicting global solar radiation (GSR) using artificial neural networks (ANN) with the most effective combination of weather variables was proposed. The study's objectives included identifying a structurally simple model for predicting solar radiation through use of an appropriate ANN to achieve better results in forecasting by reducing error values between predicted and actual data. The model used in this study combined the most effective of several weather variables in a specific location in Saudi Arabia. Historical data collected from the Solar Village in Riyadh, between 2007 and 2010, was examined to determine the influence of these weather variables: cloud-cover, relative humidity, air temperature, wind speed, wind direction, pressure and vapor on forecasting solar radiation. This data was used as an example to explore the most effective though simple model for GSR prediction. All these variables were tested through simulation and analysis using a Matlab code to model the suggested ANN structure. The optimum number of neurons for each ANN model was also determined.

In a first phase, weather variables were tested and ranked in order of effectiveness in measuring GSR. Keeping the date the same, the best results, regardless of different number of neurons applied were found with cloud cover and then relative humidity and the least effective variable was wind direction closely followed by wind speed. To

improve effectiveness, for greater accuracy and to achieve even better results, combinations of these seven variables were also tested.

Though cloud cover, humidity and temperature are the best combination of variables for predicting GSR, cloud cover is not very predictable and does not meet this study's objectives of simplicity in structure along with best results. The best combination, meeting all requirements (simplicity, good results and better accuracy in GSR prediction) was identified as air temperature, humidity and the day. This combination of variables was then evaluated for performance displayed in plots showing the predicted versus actual data and then in a further step was compared to other published models for measuring GSR. These models use different combinations of variables or more number of neurons. The proposed model fared well in comparison to published models, having a better RMSE value than even those using the same number of layers. Two models fared better using fewer neurons but they had higher RMSE. The proposed model even performed better than two different models with simpler structures as these had higher MAPE. The result of this thesis have been partially reported in [64].

6.2 Future work

This study identified the best combination of weather variables for use in a proposed model for global solar radiation (GSR) prediction that was simple in structure and used artificial neural networks. The best combination of weather variables that met the objectivities of simplicity, optimal number of neurons and better performance (as determined by r, RMSE and MAPE) was date, air temperature and relative humidity. This model fared well even when compared to previously published models using either the same weather variables or the same number of neuron network layers.

While this model performed better than published models across r, RMSE and MAPE, some of the models (Tymivios et al, 2005 and Alharbi, M (2013) used fewer neurons or had lower RMSE or MAPE. Sunshine and its duration through the day was not used as a weather variable in this study, future work can include exploring sunshine as a variable and identifying a means to address challenges of predictability that are faced when using cloud cover as a variable in GSR prediction. Codes and other mends to further simplify structure of models for GSR prediction that combine more than two variables can also be considered in further studies. Moreever, the effect of time of day and the angle of the sun radiation will be considerd.

Further investigation of the relationship between weather variables and solar radiation is recommended. Such future work could include a hybrid model for solar prediction using wavelet neural networks, and neural fuzzy network.

Bibliography

[1] British Petroleum. (July 2013). *BP Statistical Review of World Energy* [Online]. Available: http://www.bp.com/content/dam/bp/excel/Statistical-Review/statistical_review_of_world_energy_2013_workbook.xlsx.

[2] G. R. Timilsina, L. Kurdgelashvili, and P. A. Narbel, "A review of solar energy: Markets, economics and policies," The World Bank, October 2013.

[3] S. Sivanagaraju, M. R. Balasubba, and D. Srilatha, *Generation and Utilization of Electrical Energy,* India: Pearson Education, 2010.

[4] D. Anderson. (May 2013). *Solar Energy Benefits & Drawbacks* [Online]. Available: http://homeguides.sfgate.com/solar-energy-benefits-drawbacks-79613.html.

[5] W. T. Jewell, and R. Ramakumar, "The History of Utility-Interactive Photovoltaic Generation," *IEEE Trans. on Energy Conversion,* vol. 3, pp. 583-588, Sep. 1988.

[6] M. A. Green. "Photovoltaics: Comming of age," in *Proc. 21st IEEE Photov. Spec. Conf.* Kissimmee, FL, May. 1990, pp. 1-8.

[7] U.S. Department of Energy. (May 2012). *The History of Solar* [Online]. Available: http://www1.eere.energy.gov/solar/pdfs/solar_timeline.pdf.

[8] United States Environmental Protection Agency. (September 2013). *A Student's Guide to Global Climate Change - Solar Energy* [Online]. Available: http://www.epa.gov/climatestudents/solutions/technologies/solar.html.

[9] A. Luque, and S. Hegedus, *Handbook of Photovoltaic Science and Engineering,* Chichester, West Sussex, U.K.: Wiley, 2011.

[10] M. R. Pater, *Wind and Solar Power System, Design, Analysis and Operations,* Boca Raton, FL: CRC Press, 2012.

[11] N. Mohan, T. M. Undeland, and W. P. Robbins, *Power Electronics: Converters, Applications and Design,* John Wiley & Sons Australia, 2003.

[12] German Solar Energy Society, *Planning and Installing Photovoltaic Systems: A Guide for Installers, Architects and Engineers,* London, UK: Earthscan, 2008.

[13] R. A. Messenger, and J. Ventre, *Photovoltaic Systems Engineering,* Abingdon, UK: CRC Press/Taylor & Francis, 2010.

[14] N. A. Ahmed, and M. Miyatake. "A stand-alone hybrid generation system combining solar photovoltaic and wind turbine with simple maximum power point tracking control," in *Power Electronics and Motion Control Conf. (IPEMC),* Shanghai, China, 2006, pp. 1-7.

[15] A. Campoccia, S. Favuzza, E. R. Sanseverino, and G. Zizzo. "Reliability analysis of a stand-alone PV system for the supply of a remote electric load," in *Int. Symp. on Power Electronics Elect. Drives Automation and Motion, (SPEEDAM),* Pisa, Italy, June 2010, pp. 158-163.

[16] M. Musell, G. G. Notton, and A. Louche, "Design of hybrid-photovoltaic power generator, with optimization of energy management," *Solar Energy,* vol. 65, pp. 143-157, Feb. 1999.

[17] Y. Chen, C. Cheng, and H. Wu. "Grid-connected hybrid PV/wind power generation system with improved DC bus voltage regulation strategy," in *Proc. of IEEE Appl. Power Electron. Conf. and Expo. (APEC 06),* 2006, pp. 1089–1094.

[18] International Electrotechnical Commission, "Photovoltaic devices - part 3: Measurement principles for terrestrial photovoltaic (PV) solar devices with reference spectral irradiance data," 2008.

[19] A. Ruiz, "System aspects of large scale implementation of a photovoltaic power plant," M.S. thesis, School of Elect. Eng., Royal Institute of Technology, Stockholm, Sweden, 2011.

[20] H. Felten, A. Kreutzmann, and P. Welter. "Increase in grid-connected pv system power in germany," in *4th World Conf. on Photovoltaic Energy Conversion, (WCPEC-4),* Waikoloa, HI, May 2006, pp. 2494-2496.

[21] P. A. Lynn, *Electricity from Sunlight: An Introduction to Photovoltaics,* Chichester, UK: Wiley, 2010.

[22] N. K. Gautam, and N. D. Kaushika, "A Model for the Estimation of Global Solar Radiation Using Fuzzy Random Variables," *J. of Appl. Meteorology,* vol. 41, pp. 1267-1276, 2002.

[23] V. Badescu, *Modeling Solar Radiation at the Earth's Surface,* Berlin, Germany: Springer, 2008.

[24] M. J. Reno, C. W. Hansen, and J. S. Stein, "Global horizontal irradiance clear sky models: Implementation and analysis," Sandia National Laboratories, Albuquerque, NM, Tech. Rep. SAND2012-2389, Mar. 2012.

[25] METEOTEST. (March 2013). *Yearly Sum of Global Horizontal Irradiance* . Available: http://meteonorm.com/download/maps/.

[26] J. N. Black, "The distribution of solar radiation over the Earth's surface," *Theoretical and Appl. Climatology,* vol. 7, pp. 165-189, 1956.

[27] A. Hepbasli, and Z. Alsuhaibani, "A key review on present status and future directions of solar energy studies and applications in Saudi Arabia," *Renewable and Sustainable Energy Reviews,* vol. 15, pp. 5021-5050, Dec. 2011.

[28] Federal Research Division, "Country profile: Saudi arabia," Library of Congress, Sep. 2006.

[29] The world Bank. (October 2013). *Saudi Arabia* . Available: http://data.worldbank.org/country/saudi-arabia.

[30] U.S. Energy Information Administration, "Saudi arabia," U.S Energy Information Administration, Feb. 2013.

[31] F. R. Pazheri, N. H. Malik, A. A. Al-Arainy, E. A. Al-Ammar, A. Imthias, and O. K. Safoora. "Smart grid can make saudi arabia megawatt exporter," in *Asia-Pacific Power and Energy Eng. Conf., (APPEEC),* Wuhan, China, 2011, pp. 1-4.

[32] GeoModel Solar. (May 2013). *Average Annual Global Horizontal Solar Irradiation* . Available: http://solargis.info/imaps/.

[33] F. Daghestani, "Solar energy applications proceedings: Of the international seminar on appropriate technology in the fields of solar and wind energy applications," Royal Scientific Society, Amman, Jordan, 1987.

[34] M. Z. Lowenstein, and I. C. Smith. "The joint saudi arabia-united states solar energy program," in *American Inst. of Aeronautics and Astronautics, Terrestrial Energy Syst. Conf.* Orlando, Fla., June 4-6, 1979, pp. 6.

[35] W. Grasse, F. Oster, and H. Aba-Oud, "Hysolar: an overview on the German-Saudi Arabian programme on solar hydrogen," *Int. J. of Hydrogen Energy,* vol. 19, pp. 683–686, 1994.

[36] Saudi Arabia Solar Industry Association (SASIA). (December 2012). *Project Gallery* . Available: http://saudi-sia.com/?page_id=96.

[37] D. R. Myers, S. M. Wilcox, W. F. Marion, N. M. Al-Abbadi, M. bin Mahfoodh, and Z. Al-Otaibi, "Final report for annex II—Assessment of solar radiation resources in saudi arabia 1998–2000," Apr. 2002.

[38] Embassy of Switzerland-OSEC Business. (September 2012). *Saudi Arabia Major Business Sectors* . Available: http://www.s-ge.com/de/filefield-private/files/2816/field_blog_public_files/4868.

[39] National Geographic. (January 2014). *Saudi Arabia* . Available: http://travel.nationalgeographic.com/travel/countries/saudi-arabia-facts/.

[40] A. Salim, F. Huraib, and N. Eugenio. "PV power-study of system options and optimization," in *The 8th European PV SolarEnergy Conf.* Florence, Italy, 1988, .

[41] J. M. Zurada, *Introduction to Artificial Neural Networks,* St. Paul: West Publishing Company, 1992.

[42] M. Beale, M. T. Hagan and H. B. Demuth. Neural network toolbox. *The MathWorks* pp. 5-25, 2013. Available: http://www.mathworks.com.au/help/pdf_doc/nnet/nnet_ug.pdf.

[43] A. K. Jain, J. Mao and K. M. Mohiuddin. Artificial neural networks: A tutorial. *IEEE Computer 29*pp. 31-44, Mar. 1996.

[44] G. Lera, and M. Pinzolas, "Neighborhood based Levenberg-Marquardt algorithm for neural network training," *IEEE Trans. Neural Netw.,* vol. 13, pp. 1200-1203, Sep. 2002.

[45] David J Livingstone, *Artificial Neural Networks : Methods and Applications,* New York: Humana Press, vol.458, 2008.

[46] C. Voyant, P. Randimbivololona, M. L. Nivet, C. Paoli, and M. Muselli, "Twenty four hours ahead global irradiation forecasting using multi-layer perceptron," *Meteorological Applicat.,* vol. 1, Mar. 2013.

[47] A. Mellit, S. A. Kalogirou, L. Hontoria, and S. Shaari, "Artificial intelligence techniques for sizing photovoltaic systems: A review," *Renewable and Sustainable Energy Reviews,* vol. 13, pp. 406-419, 2009.

[48] J. Mubiru, and E. J. K. B. Banda, "Estimation of monthly average daily global solar irradiation using artificial neural networks," *Solar Energy,* vol. 82, pp. 181-187, 2008.

[49] A. Sözen, E. Arcaklioğlu, and M. Özalp, "Estimation of solar potential in Turkey by artificial neural networks using meteorological and geographical data," *Energy Conversion and Management,* vol. 45, pp. 3033-3052, Nov. 2004.

[50] F. S. Tymvios, C. P. Jacovides, S. C. Michaelides, and C. Scouteli, "Comparative study of Ångström's and artificial neural networks' methodologies in estimating global solar radiation," *Solar Energy,* vol. 78, pp. 752-762, Jun. 2005.

[51] S. Rehman, and M. Mohandes, "Artificial neural network estimation of global solar radiation using air temperature and relative humidity," *Energy Policy,* vol. 36, pp. 571-576, 2008.

[52] P. L. Zervas, H. Sarimveis, J. A. Palyvos, and N. C. G. Markatos, "Prediction of daily global solar irradiance on horizontal surfaces based on neural-network techniques," *Renewable Energy,* vol. 33, pp. 1796-1803, 2008.

[53] K. Moustris, A. G. Paliatsos, A. Bloutsos, K. Nikolaidis, I. Koronaki, and K. Kavadias, "Use of neural networks for the creation of hourly global and diffuse solar irradiance data at representative locations in Greece," *Renewable Energy,* vol. 33, pp. 928-932, 2008.

[54] J. C. Lam, K. K. W. Wan, and L. Yang, "Solar radiation modelling using ANNs for different climates in China," *Energy Conversion and Management,* vol. 49, pp. 1080-1090, 2008.

[55] S. Alam, S. C. Kaushik, and S. N. Garg, "Assessment of diffuse solar energy under general sky condition using artificial neural network," *Appl. Energy,* vol. 86, pp. 554-564, 2009.

[56] A. Ghanbarzadeh, A. R. Noghrehabadi, E. Assareh, and M. A. Behrang. "Solar radiation forecasting based on meteorological data using artificial neural networks," in *7th IEEE Int. Conf. on Ind. Informatics, (INDIN 2009),* 2009, pp. 227-231.

[57] A. Mellit, and A. M. Pavan, "A 24-h forecast of solar irradiance using artificial neural network: Application for performance prediction of a grid-connected PV plant at Trieste, Italy," *Solar Energy,* vol. 84, pp. 807-821, May. 2010.

[58] Fangping Deng, Gaoli Su, Chuang Liu, and Zhengxing Wang. "Global solar radiation modeling using the artificial neural network technique," in *Asia-Pacific Power and Energy Eng. Conf. (APPEEC),* 2010, pp. 1-5.

[59] Z. Wang, F. Wang, and S. Su, "Solar Irradiance Short-Term Prediction Model Based on BP Neural Network," *Energy Procedia,* vol. 12, pp. 488-494, 2011.

[60] A. Karoro, T. Ssenyonga, and J. Mubiru, "Predicting Global Solar Radiation Using an Artificial Neural Network Single-Parameter Model," *Advances in Artificial Neural Syst.,* vol. 2011, pp. 1-7, 2011.

[61] K. D. Rao, B. I. Rani, and G. S. Ilango. "Estimation of daily global solar radiation using temperature, relative humidity and seasons with ANN for indian stations," in *Int. Conf. on Power, Signals, Controls and Computation (EPSCICON),* 2012, pp. 1-6.

[62] M. Alharbi, "Daily Global Solar Radiation Forecasting Using ANN and Extreme Learning Machine: A Case Study in Saudi Arabia," M.S. thesis, Elect. and Computer Eng., Dalhousie Univ., Halifax, NS, 2013.

[63] Y. Jie, Z. Mingzhan, and W. Qinglin. "Correlative analysis of measured data between anemometer tower and WTG," in *8th Int. Conf. on Computing and Networking Technology (ICCNT),* Gueongju, 2012, pp. 111-115.

[64] B. M. Alluhaidah, S. H. Shehadeh, and M. E. El-Hawary. "Most influential variables for solar radiation forecasting using artificial neural networks," in *14th Electrical Power and Energy Conference (EPEC)*, 2014, pp. 1-5.

Appendix A. GSR Performance Evaluation with One Weather Variable

A.1 Model ANN_1.1 Performance

Table A-1 Performance Evaluation of Average Daily GSR Prediction with Cloud-Cover plus the Day

Neuron	RMSE(%)	MAPE(%)	r
40	9.6940	5.7199	0.9519
45	10.9020	6.0541	0.9451
50	10.9730	5.9039	0.9544
55	12.4050	6.4599	0.9512
60	10.1100	5.7511	0.9559
65	11.1630	5.9566	0.9509
70	10.2430	5.4365	0.9414
75	15.0340	5.6195	0.9560
80	7.1956	4.3578	0.9650
85	10.0000	5.5776	0.9444
90	9.9650	5.1166	0.9610
95	10.7200	5.2576	0.9537
100	10.2060	5.2220	0.9498
110	9.2290	4.9107	0.9630
120	10.2880	4.8691	0.9550
130	11.3330	5.0272	0.9506
140	10.6600	4.7919	0.9405
150	9.5830	4.5706	0.9501
160	12.0690	4.6884	0.9437
170	9.9880	4.6508	0.9488
180	9.6980	4.3107	0.9441
190	14.7770	5.1602	0.9198
200	8.1960	4.7822	0.9560

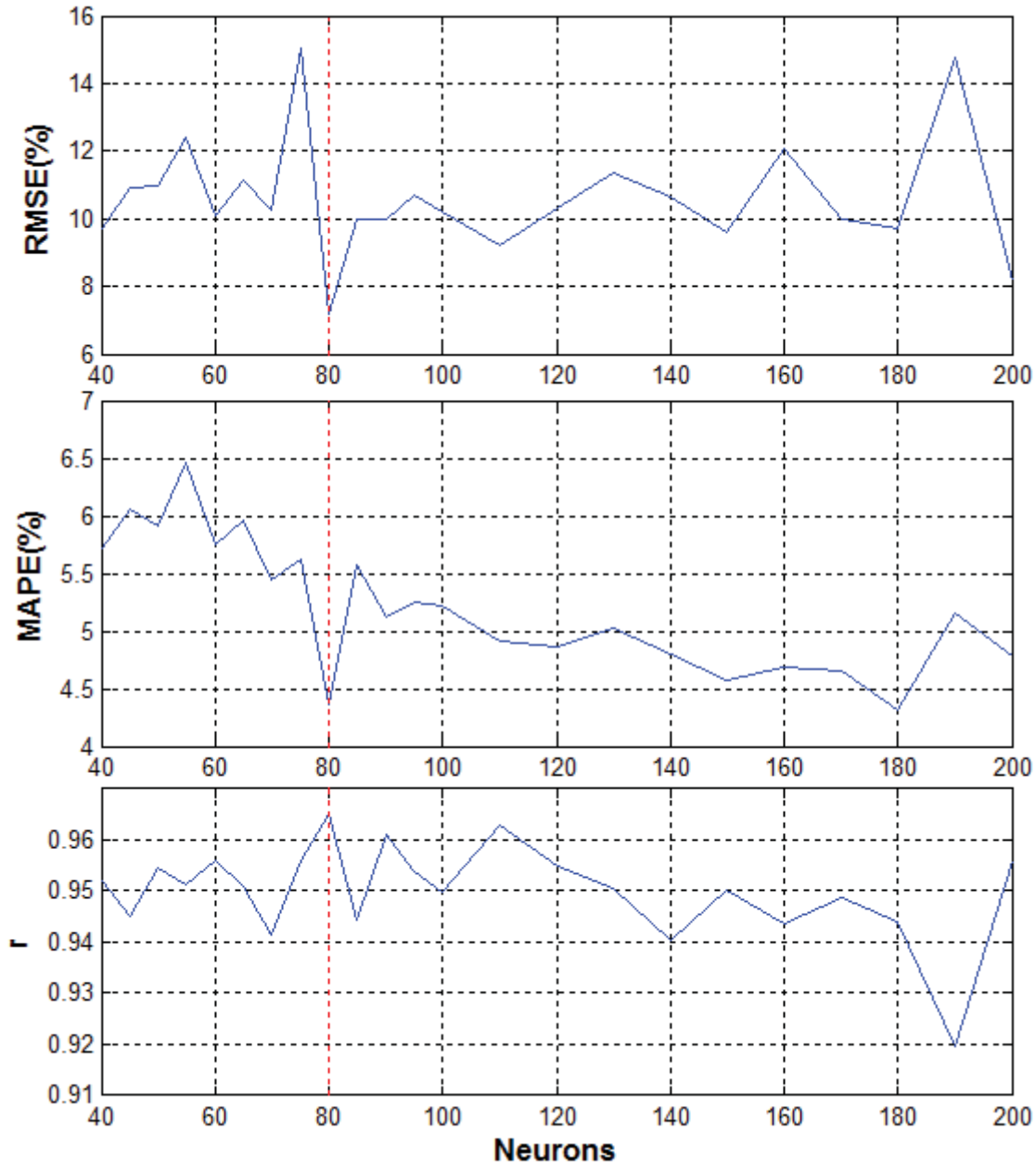

Figure A-1 Relationship between RMSE, MAPE and r with different number of neurons for Model ANN_1.1

A.2 Model ANN_1.2 Performance

Table A-2 Performance Evaluation of Average Daily GSR Prediction with Humidity plus the Day

Neuron	RMSE(%)	MAPE(%)	r
40	15.3828	7.1001	0.9397
45	15.6762	7.4087	0.9344
50	14.7294	7.1418	0.9387
55	14.5944	7.0182	0.9377
60	15.4755	7.1238	0.9375
65	14.9067	6.9982	0.9397
70	14.6232	6.5885	0.9386
75	14.0355	6.8767	0.9423
80	15.1704	6.8387	0.9407
85	14.5683	6.5724	0.9386
90	13.9383	6.6811	0.9434
95	14.2110	6.6297	0.9403
100	15.0255	6.7803	0.9377
110	13.9014	5.8959	0.9495
120	12.5865	6.0859	0.9459
130	13.6431	6.0615	0.9336
140	10.3480	5.0602	0.9502
150	13.3416	5.7773	0.9456
160	11.2482	5.3929	0.9483
170	16.1199	5.6356	0.9464
180	11.6190	5.3339	0.9420
190	12.1086	5.4815	0.9254
200	11.3949	5.2417	0.9436

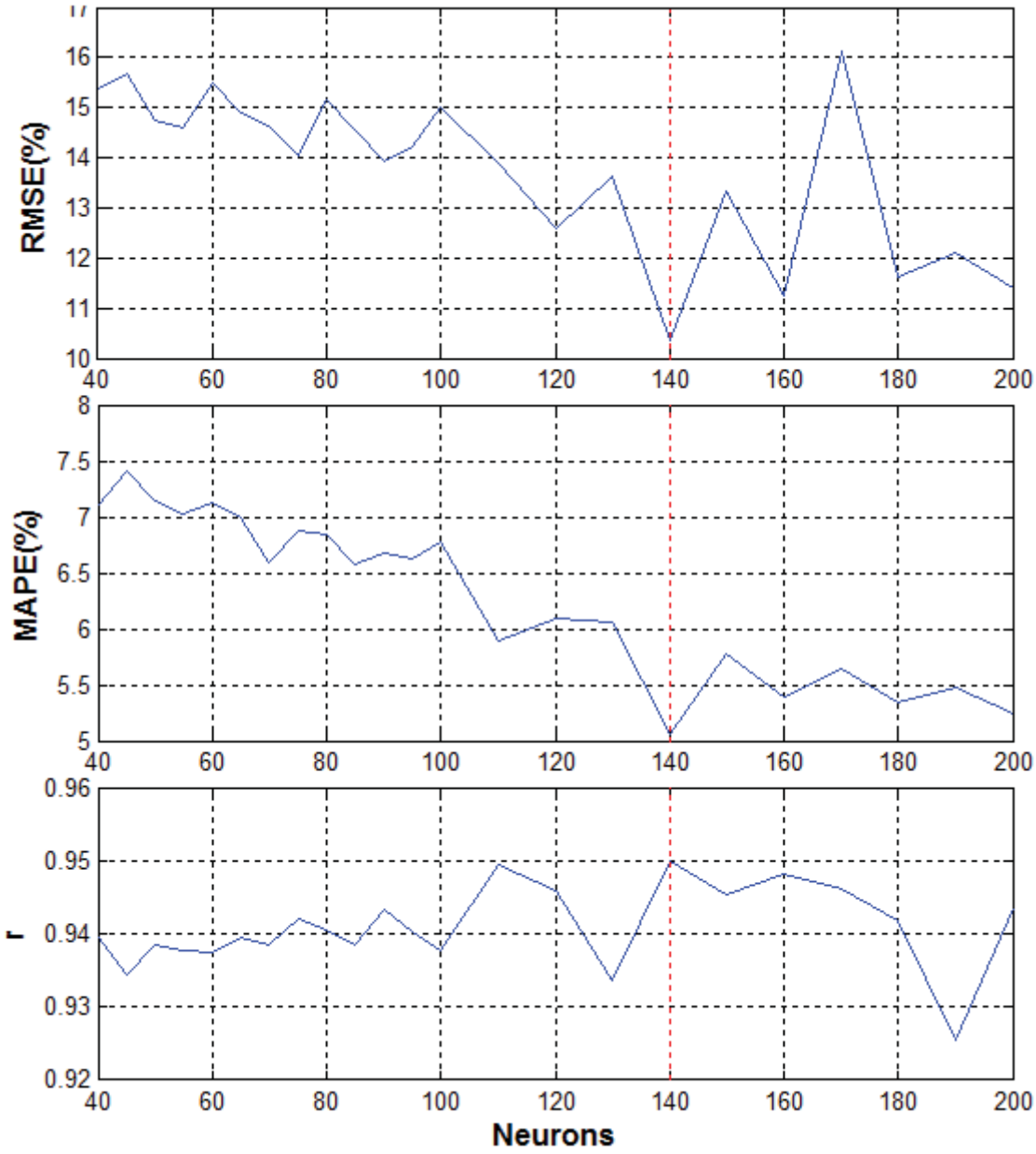

Figure A-2 Relationship between RMSE, MAPE and r with different number of neurons for Model ANN_1.2

A.3 Model ANN_1.3 Performance

Table A-3 Performance Evaluation of Average Daily GSR Prediction with Temperature plus the Day

Neuron	RMSE(%)	MAPE(%)	r
40	29.4736	8.9112	0.9139
45	22.5896	8.0226	0.9298
50	19.5744	8.1350	0.9258
55	19.2528	7.7531	0.9295
60	15.6016	7.1377	0.9422
65	17.8864	7.4788	0.9265
70	17.5384	7.4426	0.9371
75	19.7416	8.2366	0.9245
80	19.5232	8.1603	0.9237
85	23.1472	7.5281	0.9294
90	15.8752	6.9130	0.9396
95	22.8232	7.4557	0.9291
100	15.0352	7.0360	0.9272
110	34.3024	8.2243	0.9020
120	13.6224	6.5136	0.9416
131	11.916	6.0378	0.94944
140	14.9216	6.4399	0.9366
150	22.2952	6.7161	0.9348
160	17.7488	6.3364	0.9477
170	24.2488	6.9342	0.9121
180	15.7536	6.0174	0.9382
190	12.7992	5.9396	0.9352
200	13.3608	6.2299	0.9340

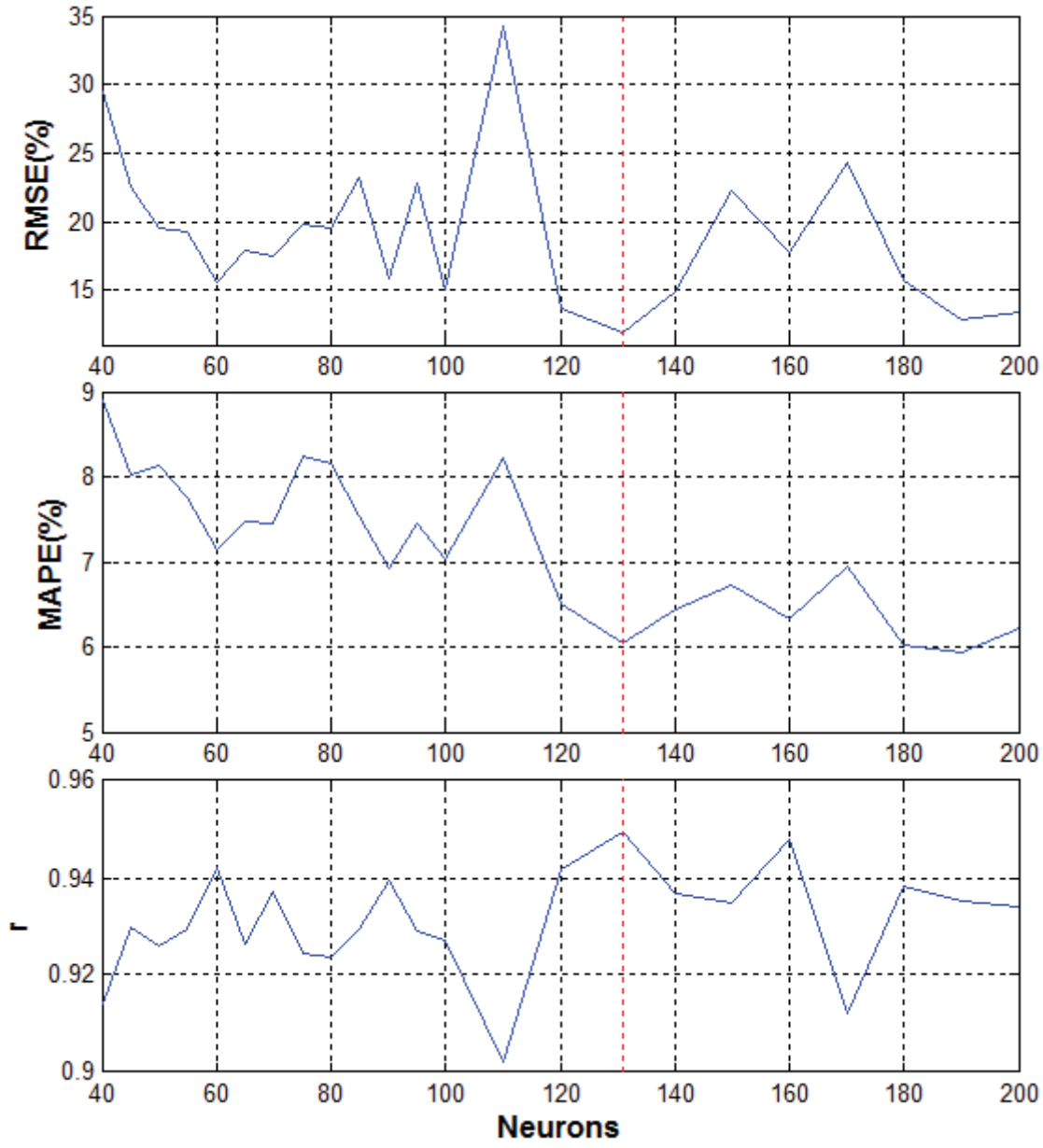

Figure A-3 Relationship between RMSE, MAPE and r with different number of neurons for Model ANN_1.3

A.4 Model ANN_1.4 Performance

Table A-4 Performance Evaluation of Average Daily GSR Prediction with Vapor plus the Day

Neuron	RMSE(%)	MAPE(%)	r
40	21.5712	9.0876	0.9154
45	22.0131	9.0097	0.9205
50	22.2111	9.0594	0.9183
55	21.2067	8.9040	0.9210
60	19.2735	8.3836	0.9255
65	21.0690	8.7970	0.9238
70	19.8819	8.5529	0.9224
75	23.8374	9.3026	0.9155
80	20.2077	8.6643	0.9237
85	15.4030	7.7645	0.9375
90	19.0782	8.3730	0.9258
95	17.5266	8.1742	0.9294
100	18.5175	8.3191	0.9269
110	17.6562	7.9863	0.9320
120	17.9442	8.0803	0.9236
130	19.2267	7.9649	0.9305
140	20.2239	8.6488	0.9245
150	16.8588	7.7254	0.9325
160	18.3042	7.8810	0.9351
170	17.2269	7.9391	0.9140
180	19.3050	7.7664	0.9304
190	15.8627	7.9180	0.9368
200	18.7272	8.0274	0.9341

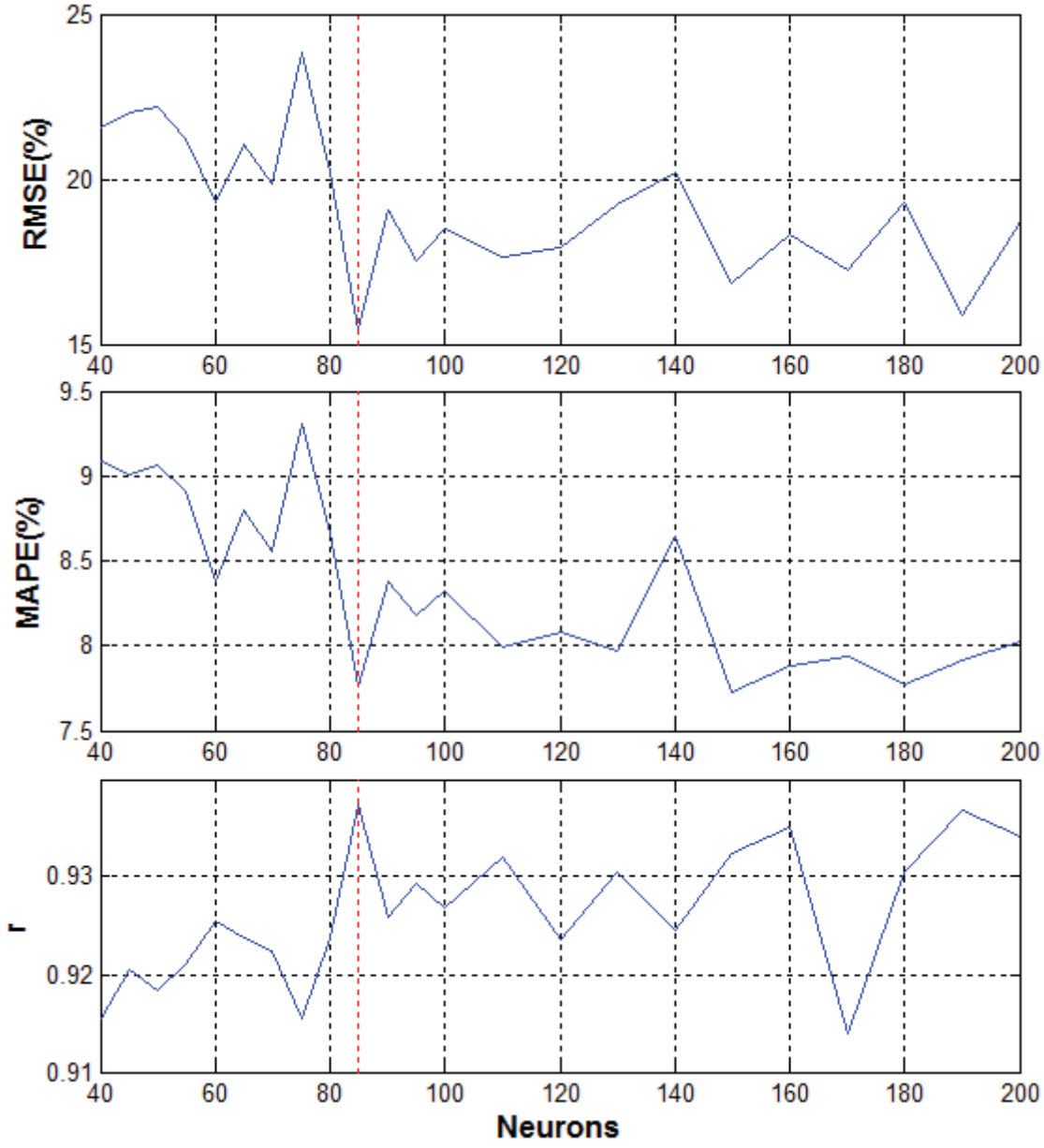

Figure A-4 Relationship between RMSE, MAPE and r with different number of neurons for Model ANN_1.4

A.5 Model ANN_1.5 Performance

Table A-5 Performance Evaluation of Average Daily GSR Prediction with Pressure plus the Day

Neuron	RMSE(%)	MAPE(%)	r
40	29.7849	10.0770	0.9010
45	30.1759	10.1452	0.9001
50	28.8703	9.6945	0.9075
55	30.5839	10.1730	0.9000
60	29.2358	9.8618	0.9053
65	29.6540	9.8018	0.9060
70	28.5864	9.6188	0.9083
75	28.2149	9.4771	0.9108
80	28.2608	9.5419	0.9082
85	28.3764	9.5236	0.9096
90	27.6973	9.3290	0.9122
95	29.3055	9.4307	0.9125
100	27.8375	9.3548	0.9134
110	28.2107	9.2758	0.9122
120	27.7993	9.3604	0.9049
130	26.1358	8.9030	0.9156
140	26.1741	9.0101	0.9150
150	24.4452	8.6024	0.9205
160	23.1720	7.9816	0.9204
170	24.5650	8.2394	0.9260
180	25.1974	8.2943	0.9234
190	24.1230	8.2706	0.9231
200	24.6653	8.2921	0.9140

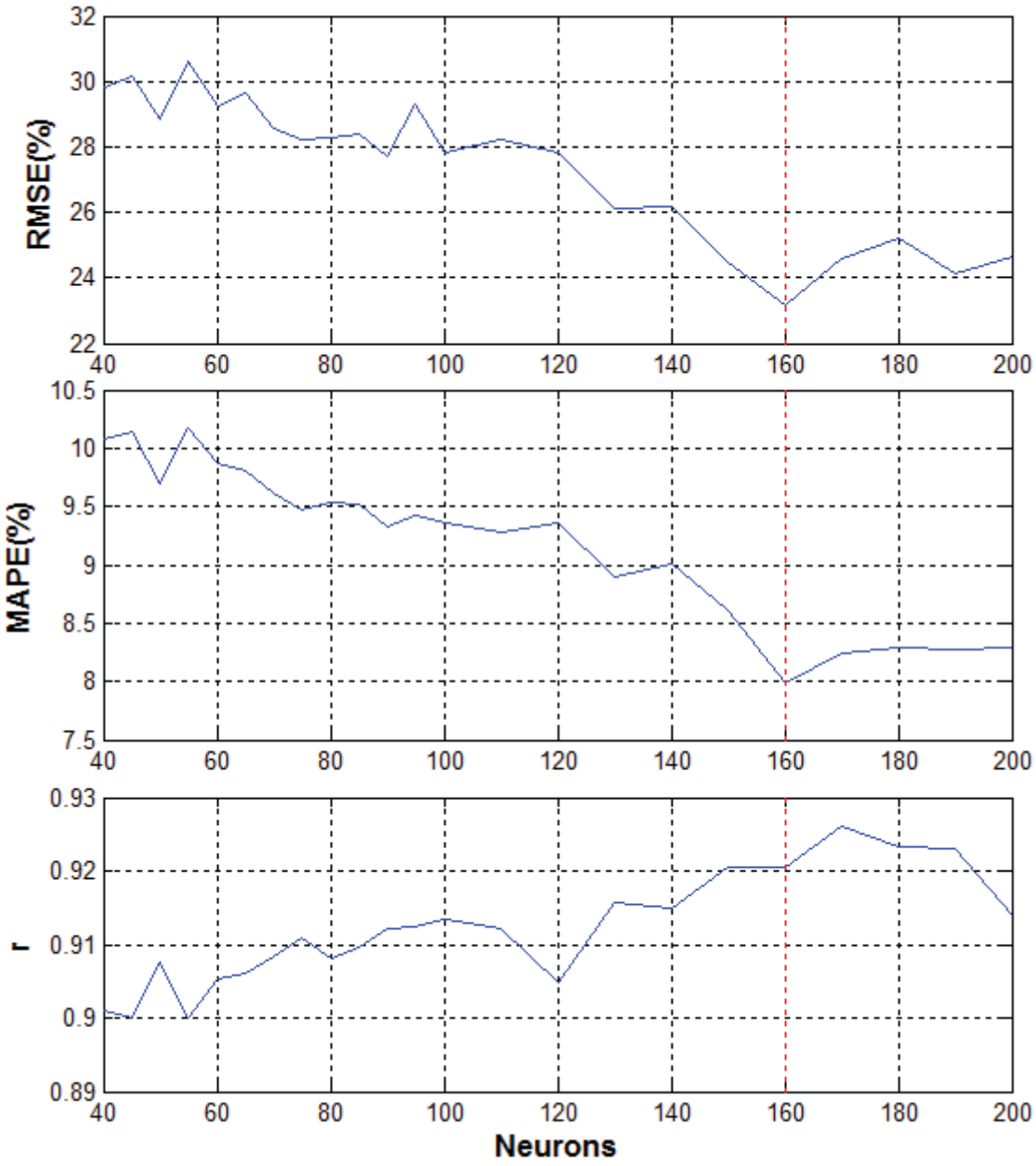

Figure A-5 Relationship between RMSE, MAPE and r with different number of neurons for Model ANN_1.5

A.6 Model ANN_1.6 Performance

Table A-6 Performance Evaluation of Average Daily GSR Prediction with Wind-Direction plus the Day

Neuron	RMSE(%)	MAPE(%)	r
40	34.779	10.4913	0.8938
45	33.245	10.5159	0.8935
50	33.739	10.5307	0.8947
55	31.829	10.1627	0.9000
60	30.738	10.2562	0.8980
65	33.845	10.6935	0.8919
70	31.366	10.181	0.9002
75	33.145	10.2752	0.8984
80	29.872	10.0409	0.8999
85	30.656	10.1507	0.8986
90	31.026	9.936	0.9014
95	33.891	10.5778	0.8939
100	27.179	9.3548	0.9067
110	28.632	9.6259	0.9035
120	29.809	9.2901	0.9109
130	30.635	9.3617	0.8999
140	27.203	9.0741	0.9107
150	34.011	9.5674	0.9063
160	27.294	8.8275	0.9124
170	27.274	8.9895	0.9094
185	25.179	8.3467	0.9018
190	25.816	8.6573	0.9042
200	30.257	9.2346	0.8821

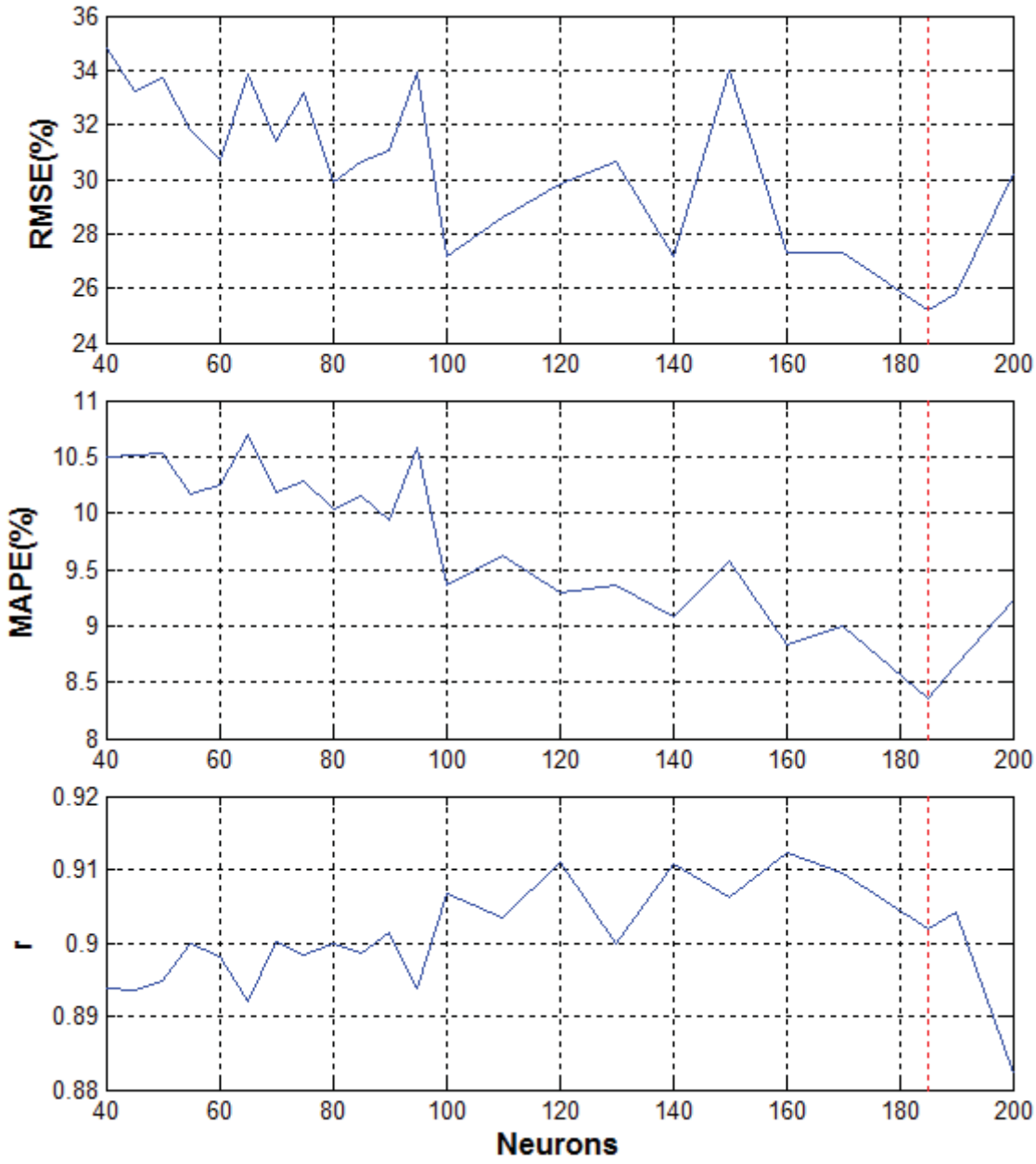

Figure A-6 Relationship between RMSE, MAPE and r with different number of neurons for Model ANN_1.6

A.7 Model ANN_1.7 Performance

Table A-7 Performance Evaluation of Average Daily GSR Prediction with Wind-Speed plus the Day

Neuron	RMSE(%)	MAPE(%)	r
40	34.7520	10.7340	0.8910
45	32.5650	10.3339	0.8961
50	34.3700	10.5577	0.8942
55	32.8380	10.4033	0.8925
60	34.1230	10.4567	0.8942
65	32.7570	10.2357	0.8975
70	32.5070	10.1827	0.8972
75	33.7400	10.0425	0.8969
80	32.3340	9.9350	0.8911
85	31.5270	9.8924	0.9019
90	32.2480	9.8933	0.8998
95	32.5900	9.8188	0.8970
100	34.0750	9.8261	0.8969
110	31.3320	9.7481	0.8951
120	32.8260	9.5919	0.9003
130	31.2160	9.6989	0.9079
140	30.5460	9.3471	0.9043
150	29.6890	9.2785	0.9002
159	27.340	8.1628	0.9084
170	29.3400	8.8891	0.9047
180	31.0820	9.6155	0.8967
190	33.3000	9.7729	0.8895
200	30.5940	9.3355	0.9015

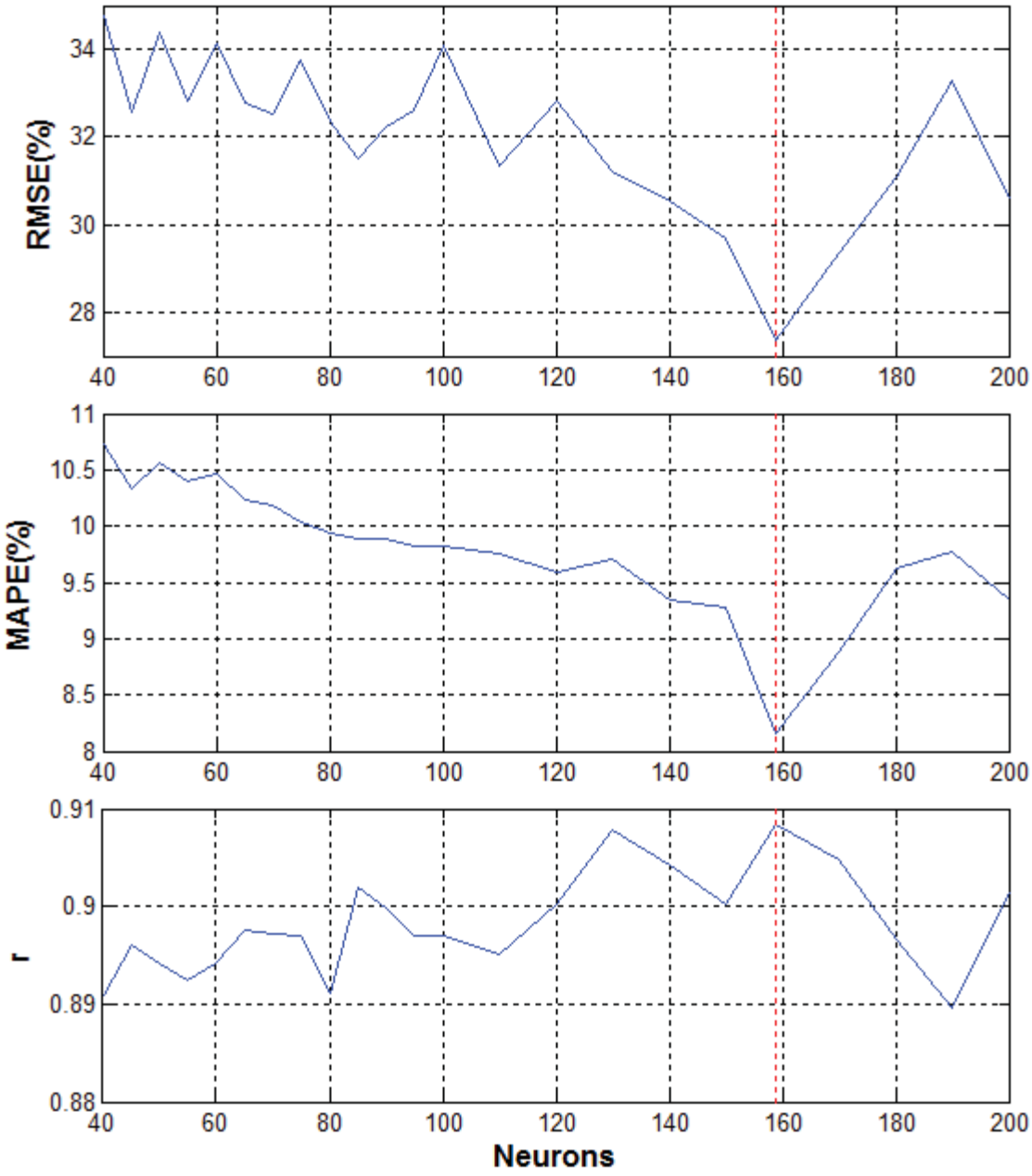

Figure A-7 Relationship between RMSE, MAPE and r with different number of neurons for Model ANN_1.7

Appendix B. GSR Performance Evaluation with Two Weather Variables

B.1 Model ANN_2.1 Performance

Table B-1 Performance Evaluation of Average Daily GSR Prediction with Humidity and Cloud-Cover plus the Day

Neuron	RMSE(%)	MAPE(%)	r
40	6.0876	4.4726	0.9690
45	5.5920	4.1714	0.9748
50	7.4556	4.7250	0.9690
55	5.9674	4.4774	0.9695
60	6.2970	4.5135	0.9698
65	6.4044	4.6091	0.9689
70	6.8640	4.7370	0.9685
75	7.0122	4.6573	0.9620
80	6.6930	4.1006	0.9706
85	4.8861	3.5358	0.9787
90	6.2424	4.6482	0.9682
95	5.0118	3.9514	0.9778
100	5.0003	3.8394	0.9759
110	5.2354	3.4717	0.9680
120	5.8931	3.4108	0.9781
130	6.0690	4.2502	0.9728
140	6.0840	4.0614	0.9763
150	5.3291	3.9857	0.9780
159	4.0337	3.1476	0.98711
170	5.3723	3.7670	0.9796
180	5.9008	4.4801	0.9710
190	5.0994	3.3726	0.9778
200	4.3553	3.4725	0.9824

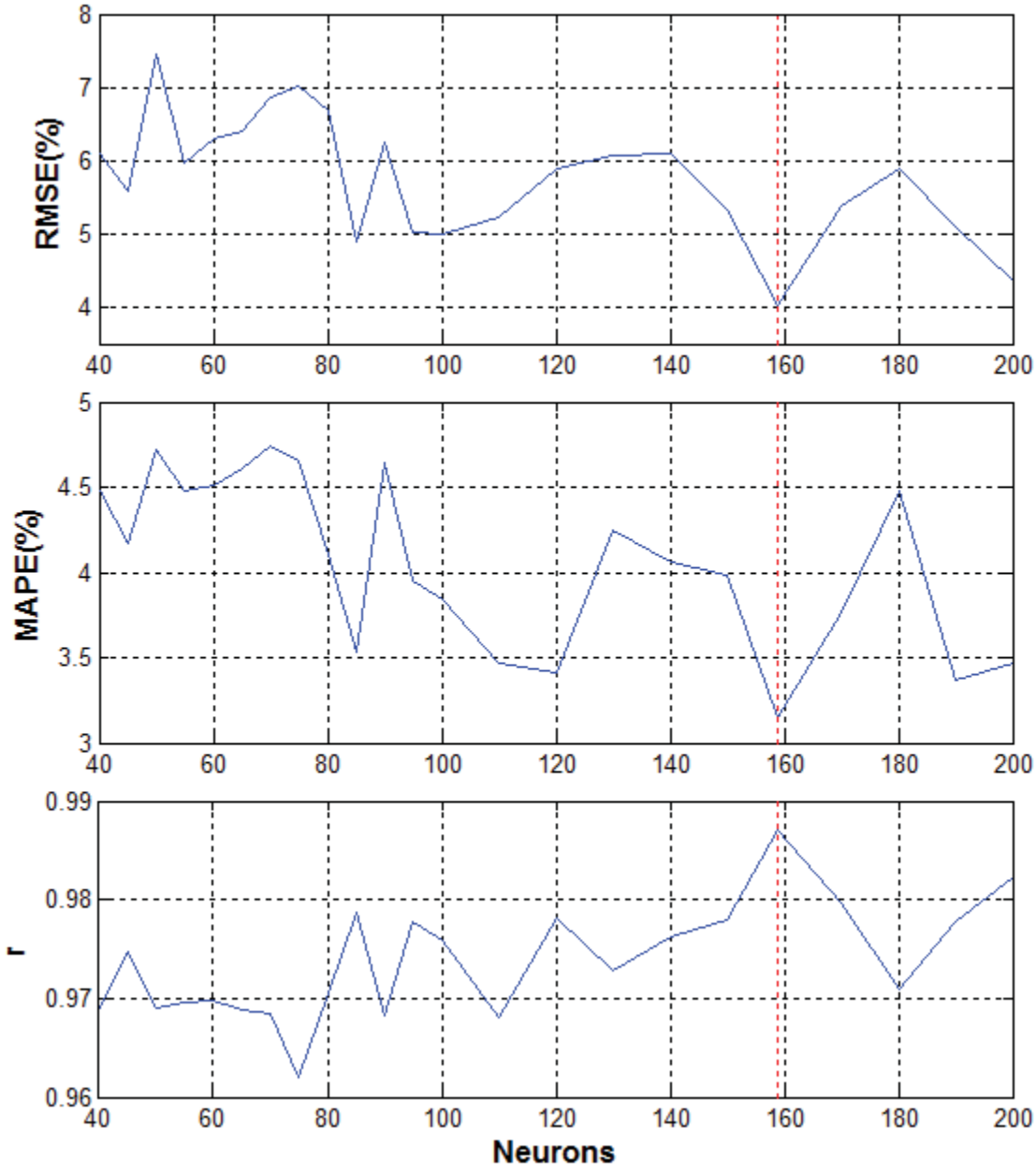

Figure B-1 Relationship between RMSE, MAPE and r with different number of neurons for Model ANN_2.1

B.2 Model ANN_2.2 Performance

Table B-2 Performance Evaluation of Average Daily GSR Prediction with Temperature and Cloud-Cover plus the Day

Neuron	RMSE(%)	MAPE(%)	r
40	5.9493	4.2747	0.9743
45	4.5855	3.7471	0.9811
50	4.9865	3.9679	0.9771
55	5.5427	3.8485	0.9800
60	5.2187	4.0552	0.9772
65	4.2822	3.4490	0.9837
70	5.5962	4.2106	0.9738
75	5.4636	4.1213	0.9755
80	5.1339	3.9533	0.9740
85	4.8696	3.9512	0.9792
90	4.8140	3.8618	0.9790
95	6.8351	4.7376	0.9635
100	4.7403	3.8596	0.9798
110	4.8250	3.8948	0.9787
120	4.9330	3.9924	0.9773
130	4.9556	4.0181	0.9764
140	4.7987	3.7447	0.9786
150	5.5167	3.7787	0.9801
160	4.4427	3.6282	0.9826
170	4.3885	3.5570	0.9849
178	4.3336	3.4697	0.9852
190	4.5096	3.5925	0.9760
200	5.0139	3.5458	0.9779

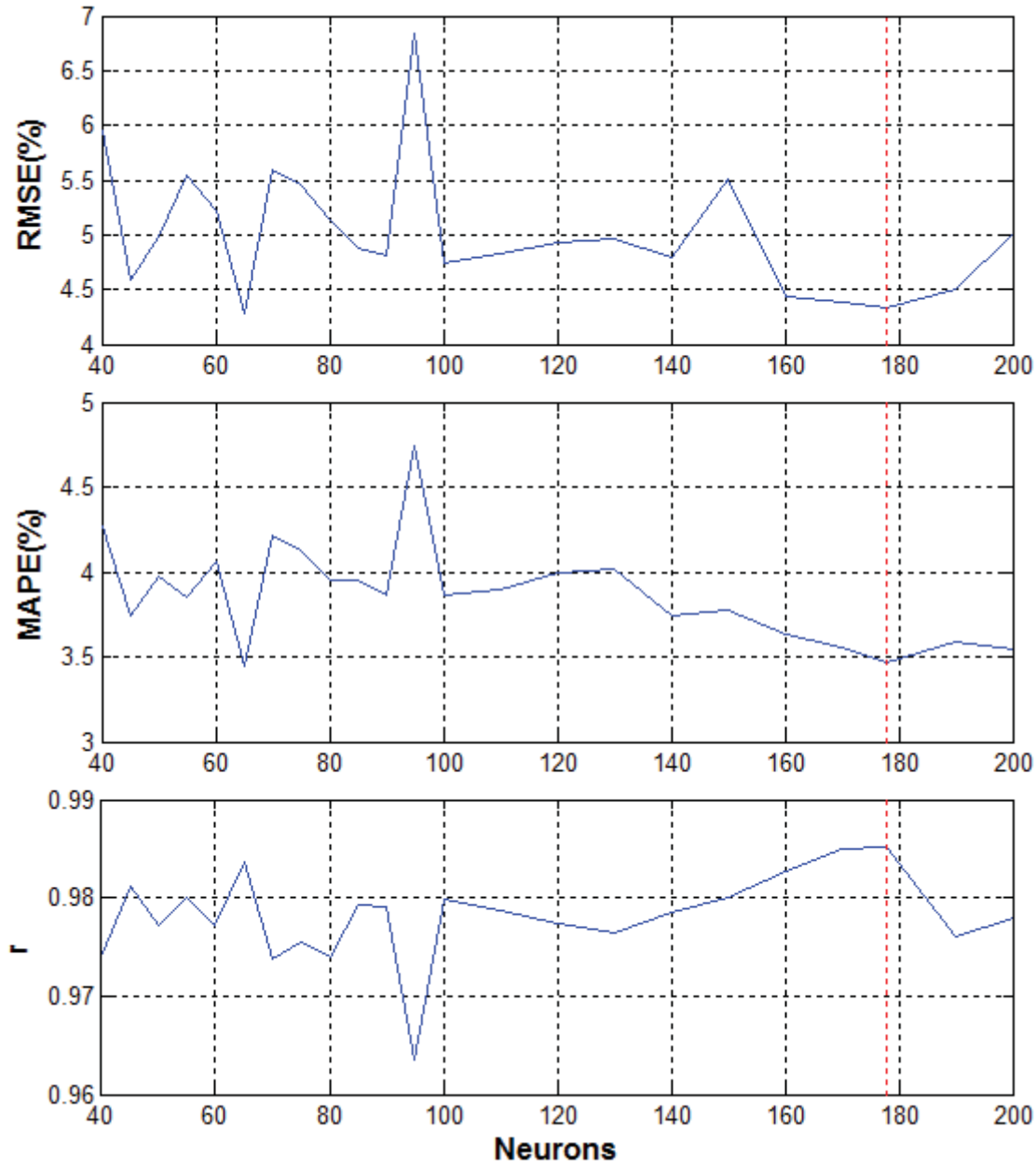

Figure B-2 Relationship between RMSE, MAPE and r with different number of neurons for Model ANN_2.2

B.3 Model ANN_2.3 Performance

Table B-3 Performance Evaluation of Average Daily GSR Prediction with Temperature and Humidity plus the Day

Neuron	RMSE(%)	MAPE(%)	r
40	6.6564	4.6885	0.9721
45	6.7667	4.8844	0.9704
50	7.1720	5.0027	0.9707
55	5.0105	4.0550	0.9774
60	7.0051	4.8880	0.9678
65	4.9742	4.0010	0.9805
70	6.5750	4.8450	0.9716
75	4.7531	3.6568	0.9802
80	6.2546	4.8400	0.9702
85	6.2947	4.7550	0.9712
90	5.6569	3.9123	0.9741
95	5.9844	4.3647	0.9709
100	5.8298	4.4440	0.9740
110	5.8857	4.5474	0.9739
120	5.7787	4.4015	0.9753
130	5.5510	3.7878	0.9741
140	4.9571	3.8858	0.9745
150	5.2289	4.0272	0.9769
160	5.8147	4.5769	0.9732
170	5.2046	4.0330	0.9795
180	6.4505	4.2016	0.9718
190	5.4037	3.7016	0.9736
200	6.1407	3.8172	0.9688

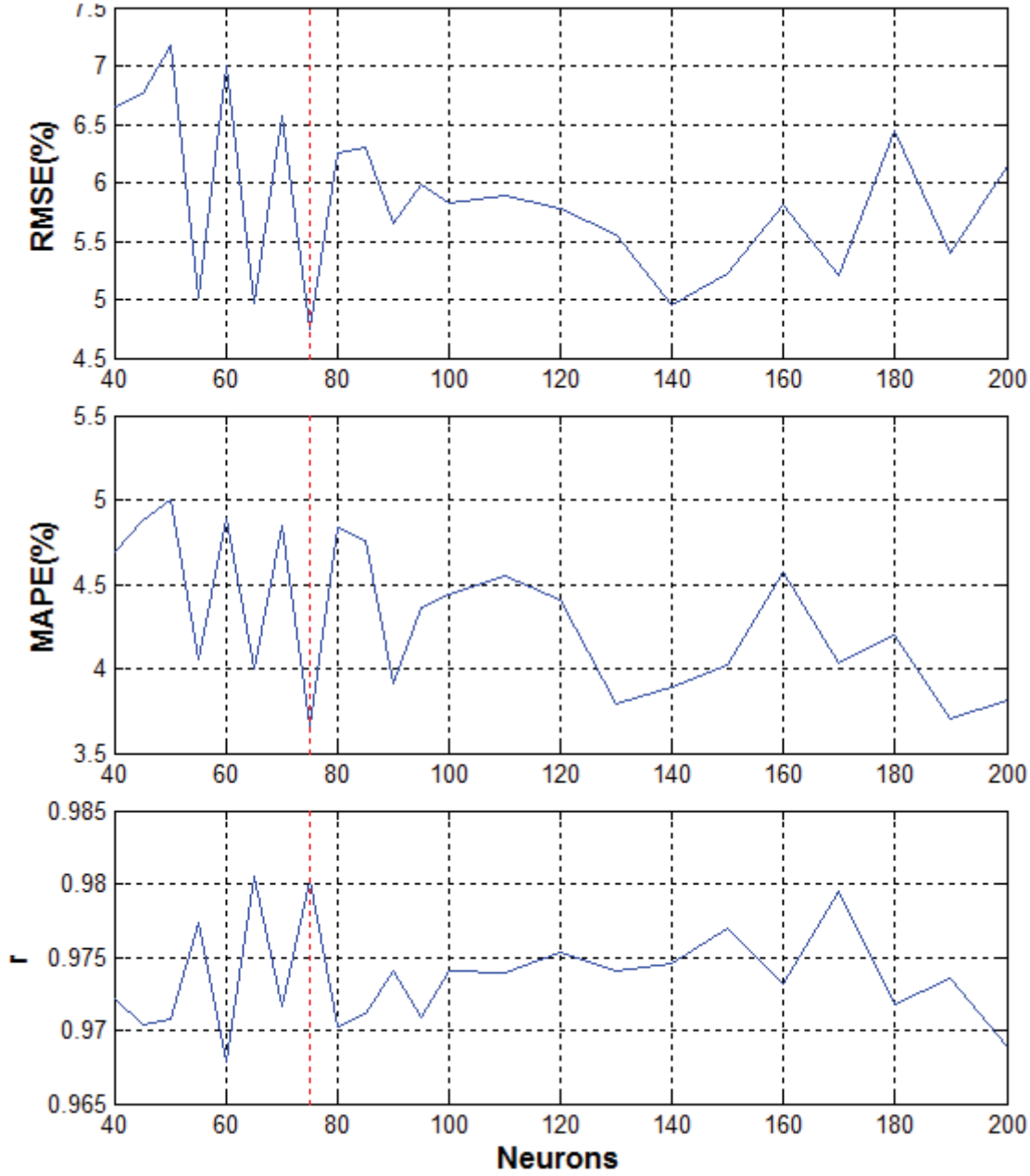

Figure B-3 Relationship between RMSE, MAPE and r with different number of neurons for Model ANN_2.3

B.4 Model ANN_2.4 Performance

Table B-4 Performance Evaluation of Average Daily GSR Prediction with Cloud-Cover and Vapor plus the Day

Neuron	RMSE(%)	MAPE(%)	r
40	8.5863	5.8192	0.9535
45	7.1557	4.9684	0.9666
50	6.9651	5.0047	0.9692
55	8.7412	5.8269	0.9538
60	8.1175	5.6506	0.9573
65	8.6536	5.3554	0.9610
70	8.2353	5.7247	0.9546
75	8.6536	5.3554	0.9610
80	10.0386	5.8777	0.9543
85	7.0864	5.1212	0.9672
90	8.0784	5.6016	0.9591
95	8.1477	5.7204	0.9553
100	5.7083	4.4828	0.9748
110	5.1025	4.1121	0.9803
115	5.1004	3.9068	0.9801
120	8.1294	5.6748	0.9552
130	8.2363	5.6209	0.9573
140	8.4685	5.7233	0.9560
150	8.3635	5.7489	0.9552
160	5.2173	4.0041	0.9769
170	6.0593	4.3779	0.9786
180	5.1450	3.8243	0.9767
190	5.5846	3.8610	0.9719
200	6.0365	4.7074	0.9728

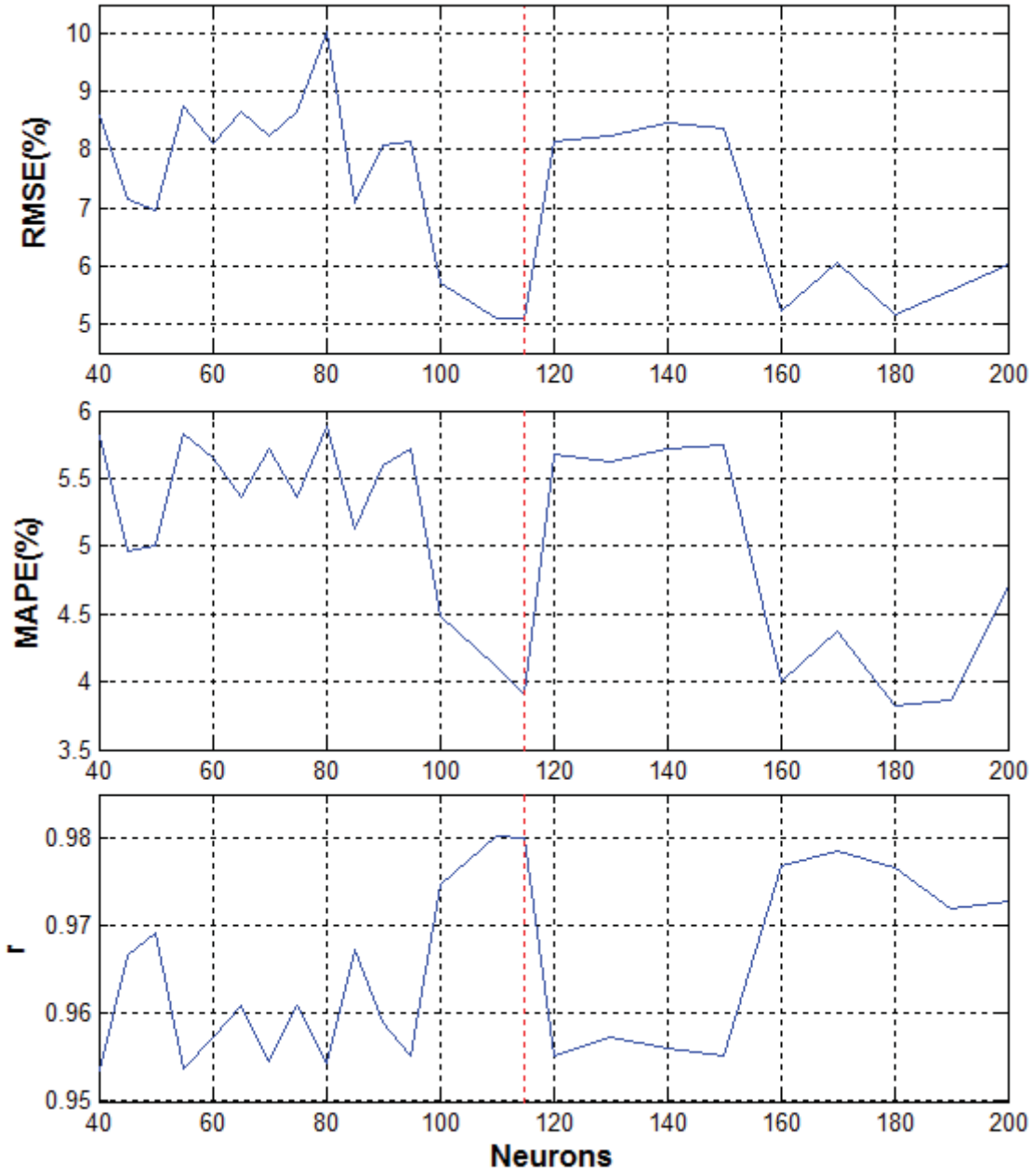

Figure B-4 Relationship between RMSE, MAPE and r with different number of neurons for Model ANN_2.4

Appendix C. GSR Performance Evaluation with More Than Two Weather Variables

C.1 Model ANN_3.1 Performance

Table C-1 Performance Evaluation of Average Daily GSR Prediction with Temperature, Humidity, Cloud-Cover and Vapor plus the Day

Neuron	RMSE(%)	MAPE(%)	r
40	5.6287	3.9101	0.9782
45	5.2175	3.5793	0.9817
50	5.2951	3.6484	0.9795
55	5.8025	3.8190	0.9802
60	6.2202	3.9396	0.9773
65	4.9205	3.0878	0.9818
70	6.5664	4.2263	0.9750
75	6.3042	3.9268	0.9776
80	5.4828	3.5775	0.9841
85	6.1836	4.0090	0.9794
90	5.7491	3.8746	0.9795
95	6.4404	4.1406	0.9767
100	6.7194	3.1003	0.9761
110	6.7500	4.1418	0.9770
120	6.3426	4.0439	0.9755
130	6.7368	4.2152	0.9768
140	4.0943	2.7580	0.9900
150	4.9856	3.3845	0.9837
160	3.4764	2.2557	0.9920
170	4.8135	2.7523	0.9876
180	4.2650	2.7253	0.9870
190	5.2008	3.2802	0.9845
200	4.6799	3.0905	0.9850

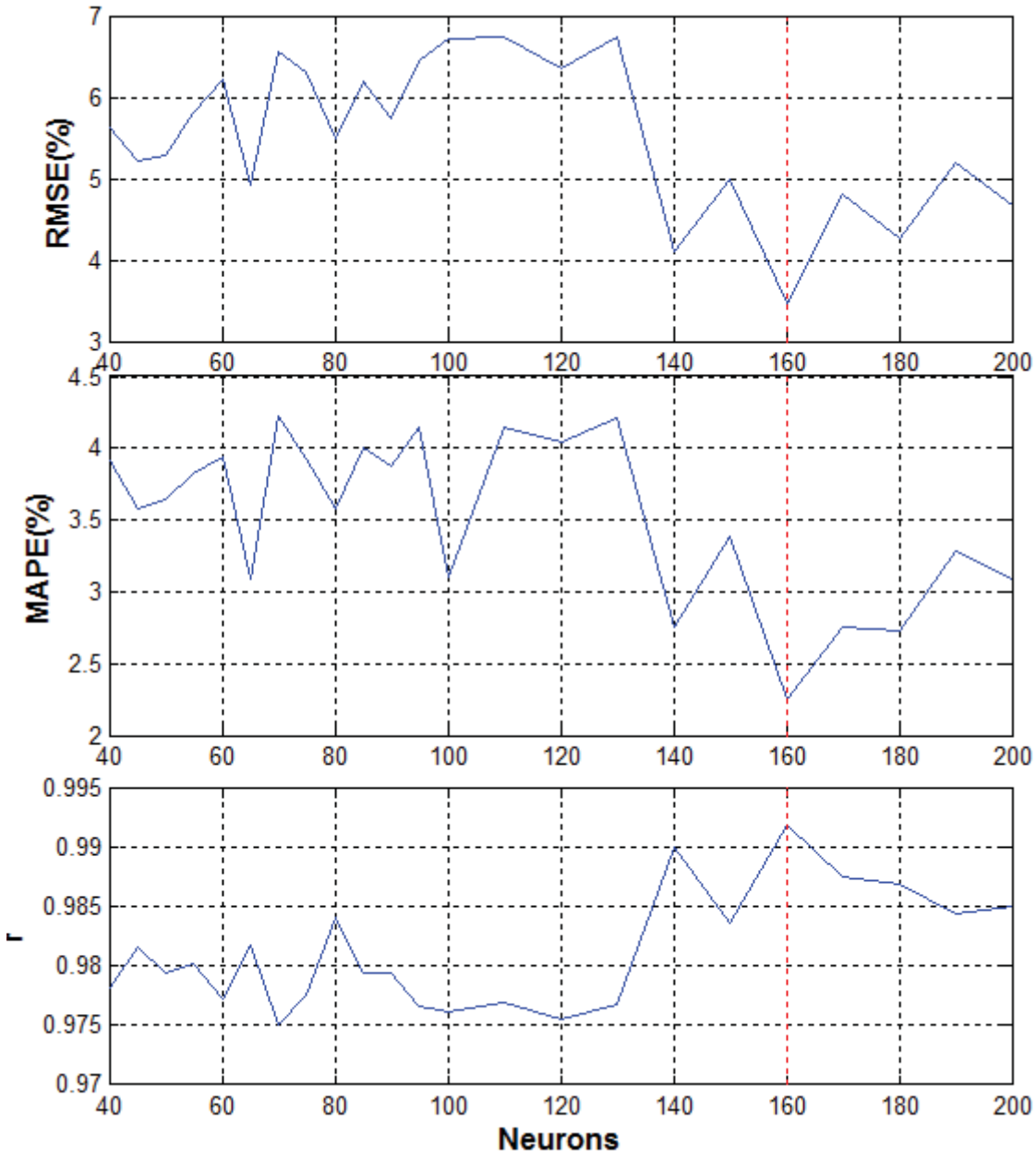

Figure C-1 Relationship between RMSE, MAPE and r with different number of neurons for Model ANN_3.1

C.2 Model ANN_3.2 Performance

Table C-2 Performance Evaluation of Average Daily GSR Prediction with Temperature, Humidity and Cloud-Cover plus the Day

Neuron	RMSE(%)	MAPE(%)	r
40	5.3840	3.7912	0.9764
45	5.5154	3.9713	0.9680
50	4.6396	3.3754	0.9814
55	4.5186	3.4196	0.9828
60	4.4372	3.2069	0.9852
65	3.8191	2.9510	0.9891
70	5.4553	3.7514	0.9769
75	4.3403	3.2705	0.9832
80	5.2076	3.7526	0.9776
85	4.2964	3.0204	0.9870
90	4.7310	3.1258	0.9828
95	5.3308	3.7948	0.9781
100	4.6190	3.3952	0.9829
110	5.4226	3.8064	0.9786
120	5.2792	3.7656	0.9792
130	5.7536	3.8757	0.9765
140	5.3167	3.5765	0.9816
150	4.5958	3.0998	0.9853
160	5.4715	3.9433	0.9745
170	4.6555	2.9257	0.9823
180	4.8844	2.8573	0.9879
190	4.6862	2.7305	0.9851
200	4.1356	3.0979	0.9871

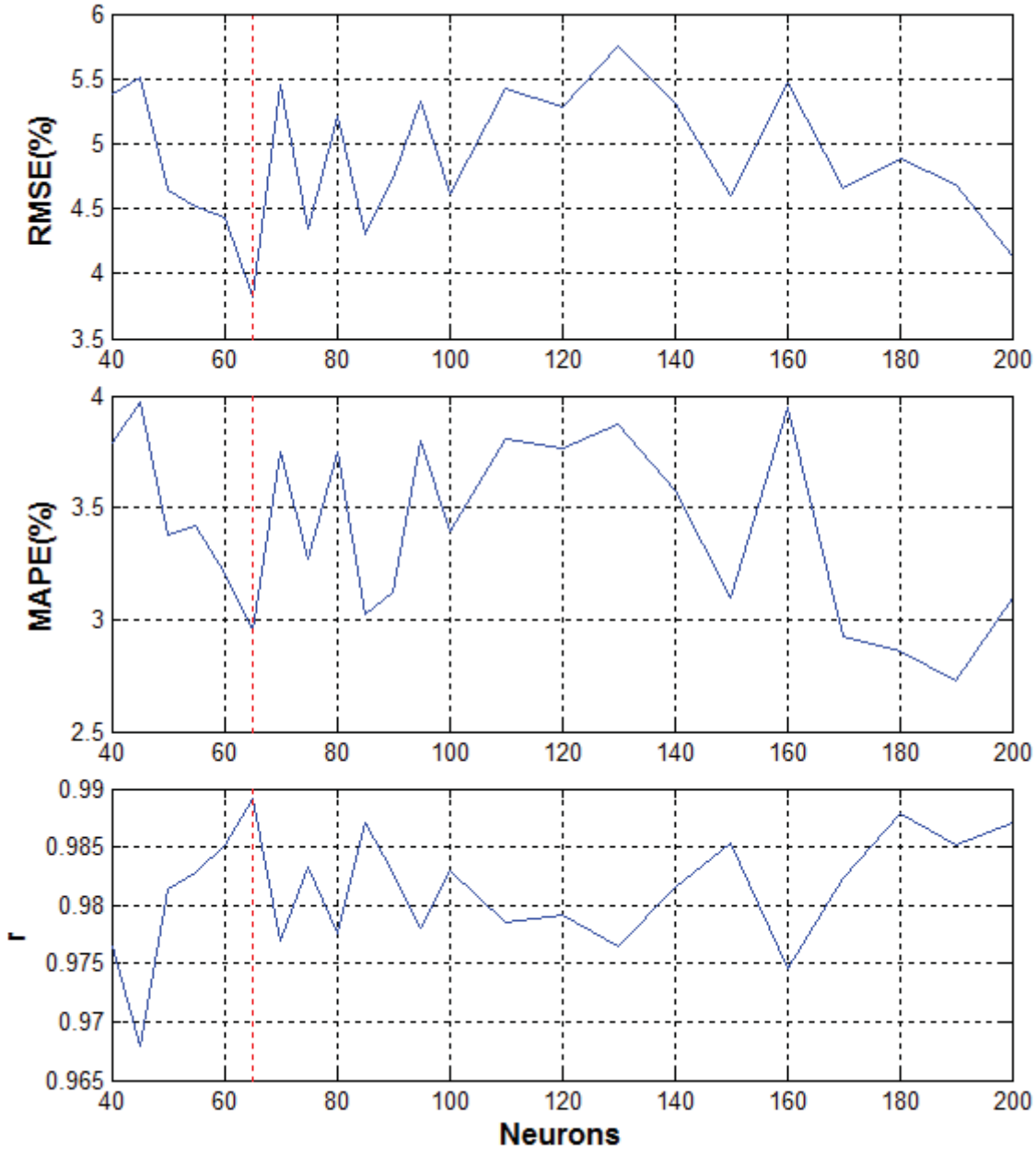

Figure C-2 Relationship between RMSE, MAPE and r with different number of neurons for Model ANN_3.2

Appendix D. Performance Evaluation of Proposed Model

D.1 Sub-Model I Performance

Table D-1 Performance Evaluation of Average Daily GSR Prediction with Temperature and Humidity plus the Day

Neuron	RMSE(%)	MAPE(%)	r
40	6.6564	4.6885	0.9721
45	6.7667	4.8844	0.9704
50	7.1720	5.0027	0.9707
55	5.0105	4.0550	0.9774
60	7.0051	4.8880	0.9678
65	4.9742	4.0010	0.9805
70	6.5750	4.8450	0.9716
75	4.7531	3.6568	0.9802
80	6.2546	4.8400	0.9702
85	6.2947	4.7550	0.9712
90	5.6569	3.9123	0.9741
95	5.9844	4.3647	0.9709
100	5.8298	4.4440	0.9740
110	5.8857	4.5474	0.9739
120	5.7787	4.4015	0.9753
130	5.5510	3.7878	0.9741
140	4.9571	3.8858	0.9745
150	5.2289	4.0272	0.9769
160	5.8147	4.5769	0.9732
170	5.2046	4.0330	0.9795
180	6.4505	4.2016	0.9718
190	5.4037	3.7016	0.9736
200	6.1407	3.8172	0.9688

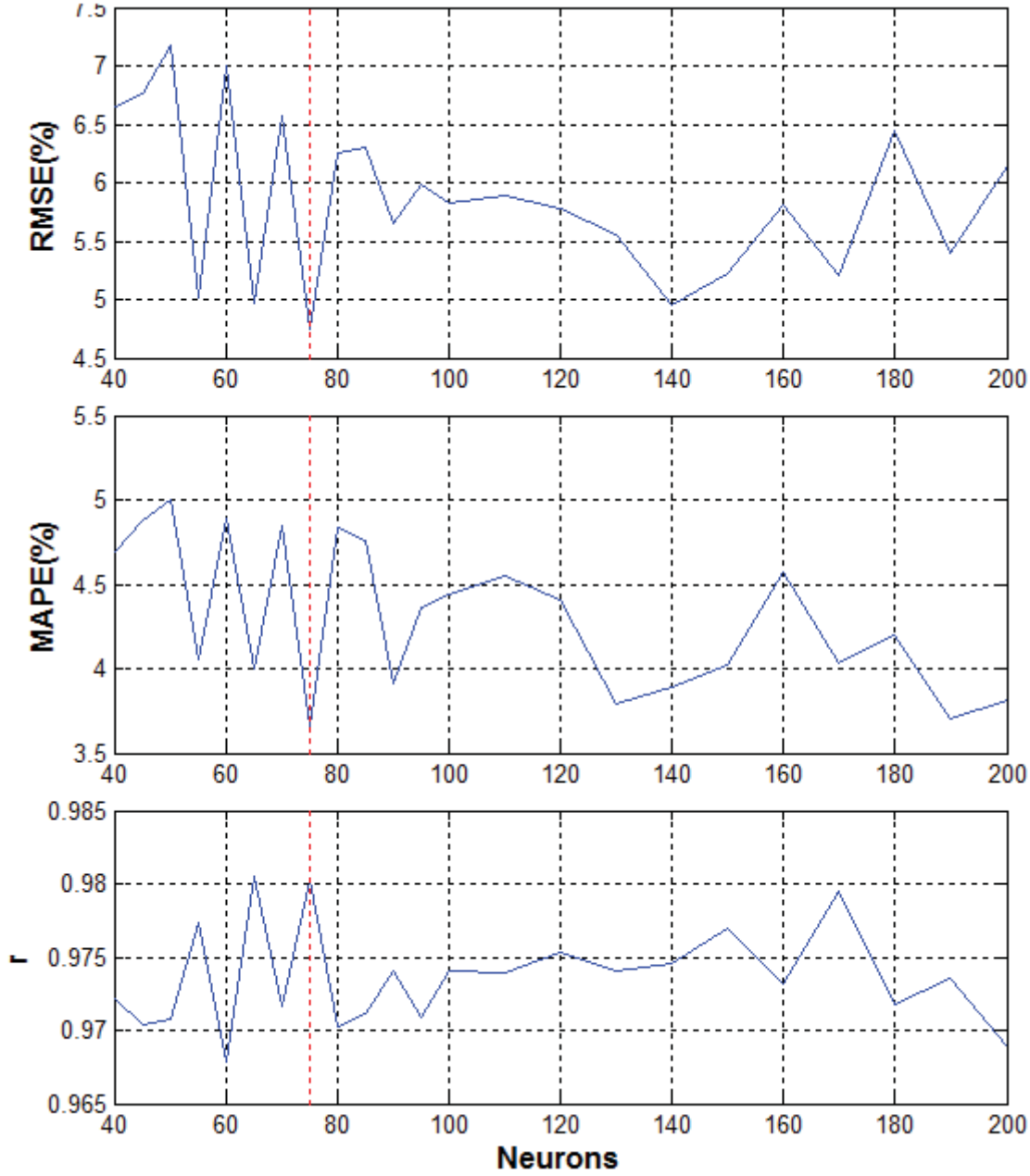

Figure D-1 Relationship between RMSE, MAPE and r with different number of neurons for Sub-Model I.

D.2 Sub-Model II Performance

Table D-2 Performance Evaluation of Average Daily Temperature with Temperature, Humidity and GSR Plus the Day

Neuron	RMSE(%)	MAPE(%)	r
40	14.4094	8.8171	0.9524
45	14.5778	8.7322	0.9583
50	14.2513	8.6457	0.9536
55	13.0088	7.8180	0.9562
60	12.5411	7.4841	0.9603
65	13.7408	8.2970	0.9559
70	13.9054	8.4294	0.9541
75	14.8512	8.6673	0.9582
80	14.1081	8.3471	0.9553
85	14.4531	8.4364	0.9570
90	15.8519	8.8881	0.9583
95	12.7382	7.6144	0.9596
100	15.0809	8.7192	0.9587
110	11.3981	6.6460	0.9492
120	11.6036	6.5778	0.9512
130	12.2146	7.3594	0.9559
140	12.7587	7.1279	0.9587
151	10.715	6.3407	0.9626
160	12.6713	7.2430	0.9597
170	16.2053	9.0815	0.9570
180	16.2118	8.8874	0.9567
190	16.6386	9.2962	0.9556
200	15.3841	8.9339	0.9578

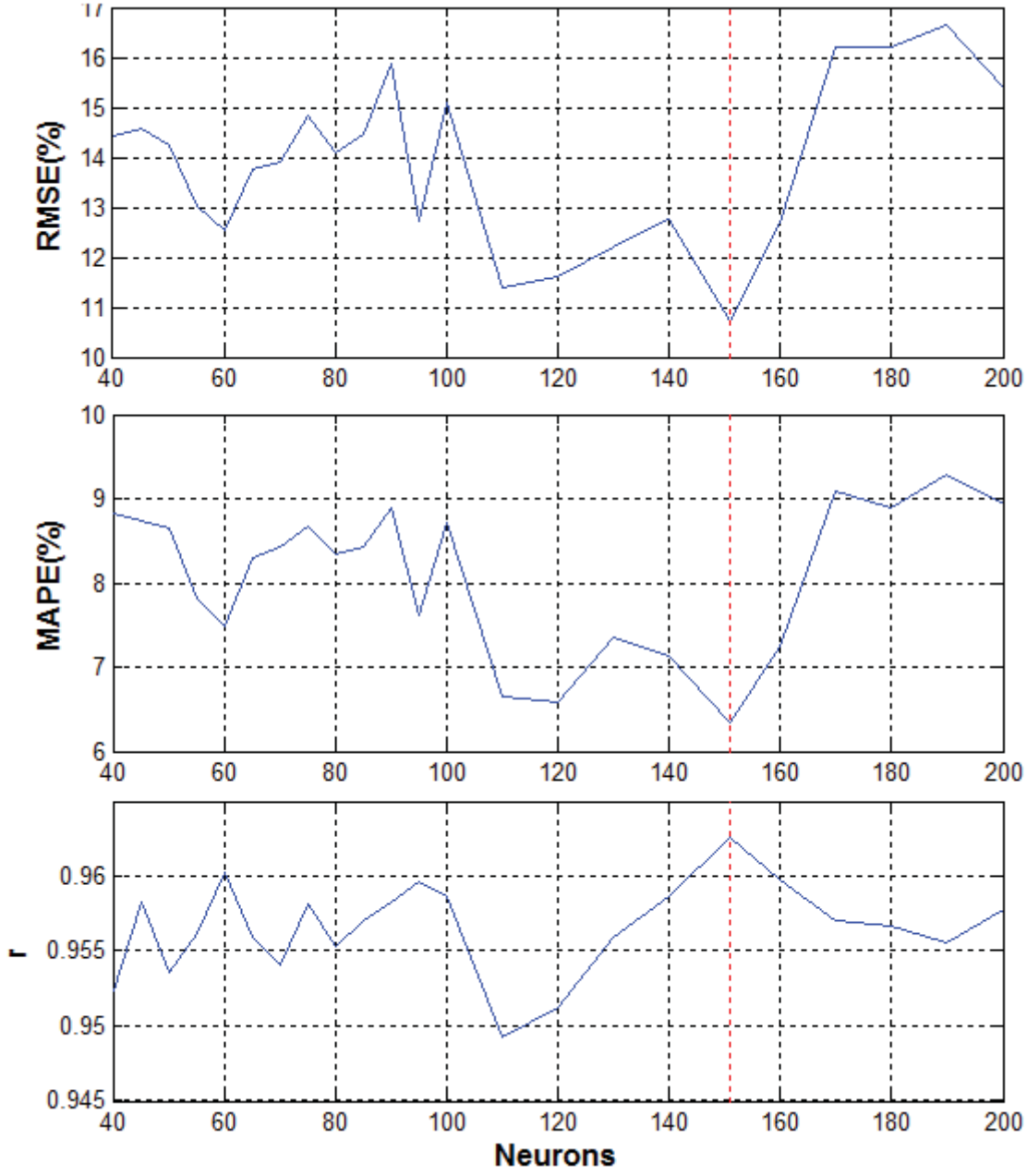

Figure D-2 Relationship between RMSE, MAPE and r with different number of neurons for Sub-Model II

D.3 Sub-Model III Performance

Table D-3 Performance Evaluation of Average Daily Humidity with Temperature, Humidity and GSR Plus the Day

Neuron	RMSE(%)	MAPE(%)	r
40	19.7168	12.1398	0.9260
45	20.0784	12.2881	0.9250
50	18.8240	11.6536	0.9358
55	20.8168	12.7585	0.9116
60	20.8288	12.5136	0.8823
65	21.2680	12.4275	0.8912
70	17.9208	10.9353	0.9339
75	19.0888	11.4853	0.9378
80	20.7336	12.5480	0.9165
85	17.4424	10.7503	0.9264
90	18.7696	11.2662	0.9340
95	19.4424	11.3288	0.9283
100	21.8200	10.7699	0.9000
110	19.4488	10.3625	0.9145
120	22.1296	12.9205	0.8773
130	20.3272	10.4948	0.9201
135	15.0090	9.0621	0.9444
140	16.0072	9.7435	0.9401
150	18.7848	10.3434	0.9314
160	19.6008	10.5858	0.9399
170	21.1112	11.2946	0.9075
180	21.8480	11.0830	0.9211
190	20.9688	10.5813	0.8932
200	20.3632	11.1242	0.9012

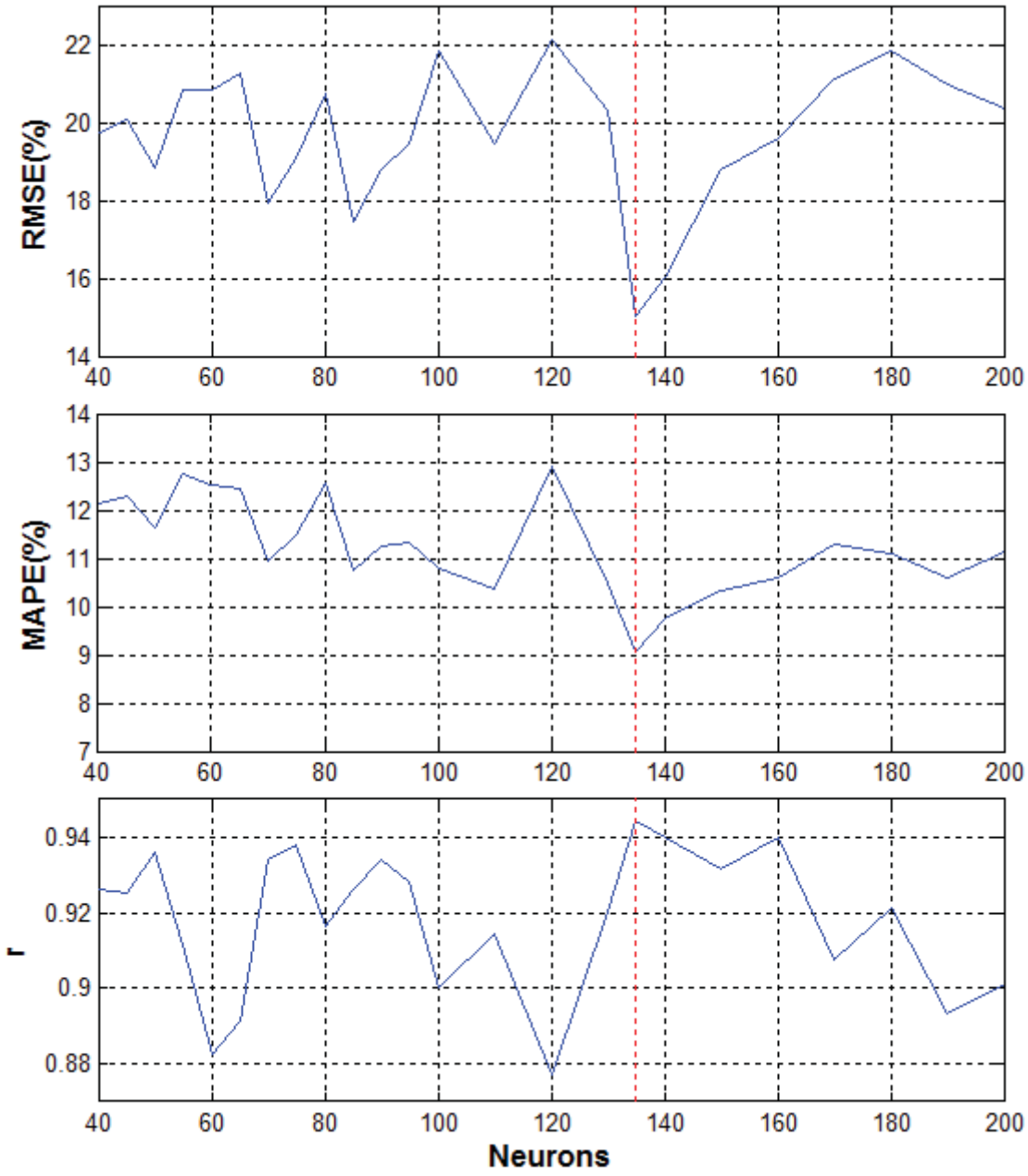

Figure D-3 Relationship between RMSE, MAPE and r with different number of neurons for Sub-Model III

D.4 Sub-Model IV Performance

Table D-4 Performance Evaluation of Average Daily Humidity with Temperature, Humidity and GSR Plus the Day

Neuron	RMSE(%)	MAPE(%)	r
40	10.8140	8.2888	0.9084
45	10.8234	8.3314	0.9213
50	10.6886	7.9950	0.9263
55	10.6035	7.7930	0.9231
60	10.7409	7.8947	0.9301
65	7.9714	6.5614	0.9264
70	9.4569	7.6110	0.9140
75	9.5401	7.2580	0.9188
80	9.7889	6.8443	0.9178
85	11.3784	7.2449	0.9272
90	11.2461	7.8787	0.9088
95	10.8392	7.1671	0.9183
100	8.1755	6.1591	0.9207
110	7.8416	5.8747	0.9292
115	7.1492	6.0868	0.9389
120	7.9078	6.1049	0.9305
130	8.4326	6.2741	0.9211
140	8.6379	6.7752	0.9205
150	10.4838	5.9766	0.9290
160	10.8896	6.7804	0.9140
170	7.8555	6.2773	0.9148
180	8.2366	5.8456	0.9173
190	8.1711	6.5330	0.9234
200	10.4769	7.9873	0.9228

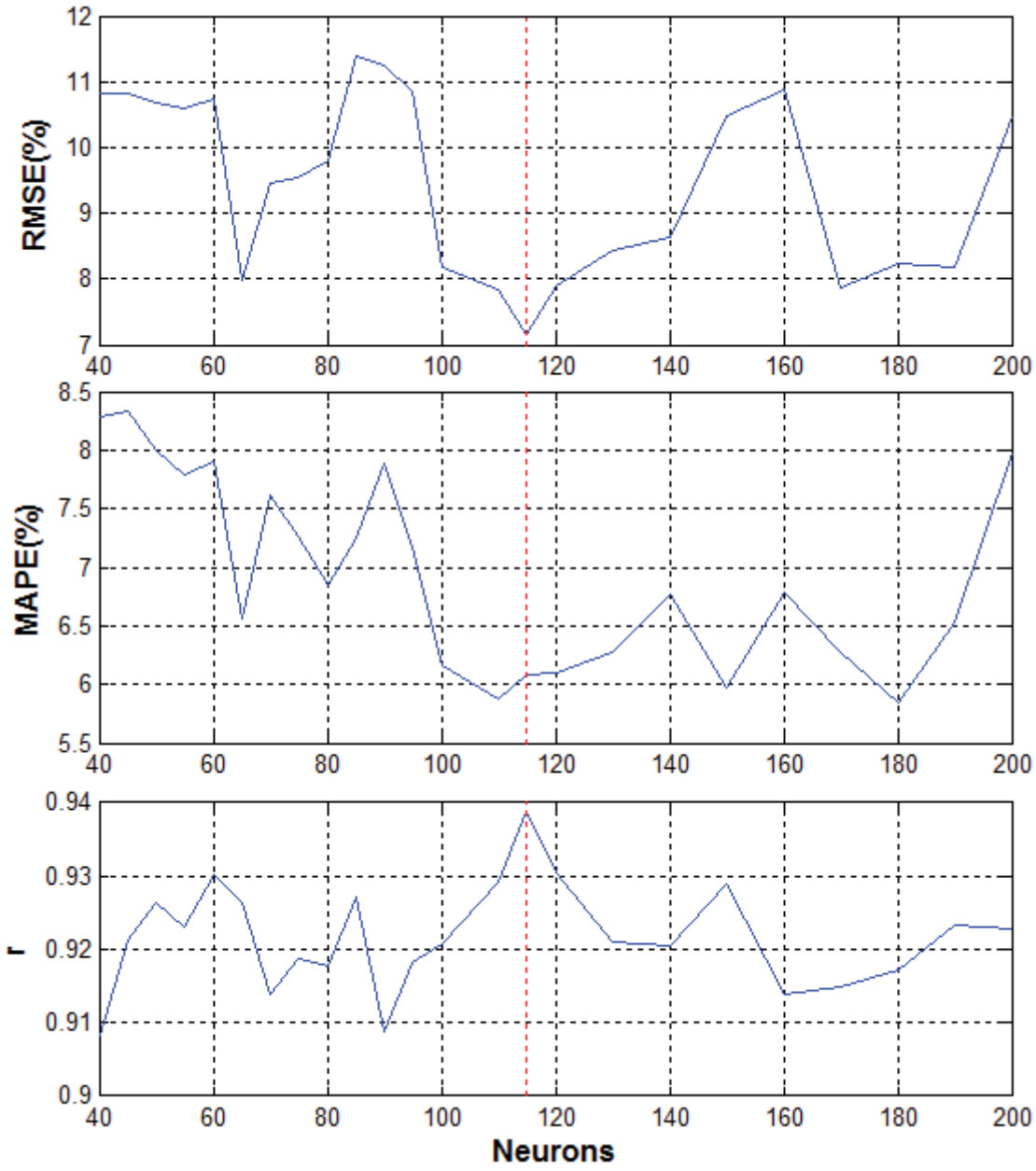

Figure D-4 Relationship between RMSE, MAPE and r with different number of neurons for Sub-Model IV